Applied Catalysis B: Environmental 341 (2024) 123253

Contents lists available at ScienceDirect

Applied Catalysis B: Environmental

journal homepage: www.elsevier.com/locate/apcatb

Impact of Mg on Pd-based methane oxidation catalysts for lean-burn natural gas emissions control☆

Sreshtha Sinha Majumdar *, Melanie Moses-DeBusk *, Dhruba Jyoti Deka, Michelle K. Kidder, Calvin R. Thomas, Josh A. Pihl

National Transportation Research Center, Oak Ridge National Laboratory, Knoxville, TN 37932, USA

ARTICLE INFO

Keywords:
Methane oxidation
MOC
Catalyst
Light-off
Natural gas
Lean burn
Palladium catalyst
Magnesium
Alumina
Zeolite

ABSTRACT

More efficient lean-burn, natural gas engines are limited by greenhouse gas emissions due to methane oxidation catalysts (MOC) that suffer from water inhibition and high temperature activation. Herein, we report that the addition of Mg to supported 1 wt% Pd MOCs improved hydrothermal stability even after severe hydrothermal aging. The superior methane oxidation activity compared to the corresponding Mg-free catalyst was attributed to (1) influence of Mg during surface roughening and restructuring at 700 °C on metal-support interaction, (2) reducibility of PdOx sites and (3) preferential stabilization of active Pd (1 0 0) facets in the sample as was evidenced by H_2 TPR and CO TPD characterization experiments. Methane conversion under synthetic exhaust conditions relevant to natural gas, lean-burn engines were investigated. BET, TPR, CO pulse chemisorption followed by TPD provided valuable insights into the surface area, pore volume, reducibility, Pd dispersion and Pd particle size of the selected catalyst samples.

1. Introduction

Natural gas has garnered tremendous attention as an alternative to traditional fossil fuels due to its abundance, cost-effectiveness and versatility of use in the transportation, power generation, marine and manufacturing sectors [1–4]. Methane, the primary component of natural gas, has lower carbon content and emits less CO_2 per unit energy generated compared to other carbon-intensive fossil fuels [2,5–7]. Furthermore, natural gas-fueled, lean-burn engines operating under high air-to-fuel ratios ($\lambda > 1$) have better thermal efficiencies, can reduce fuel consumption, and have lower engine-out pollutant emissions than conventional stoichiometric engines [8–10]. However, exhaust streams from natural gas, lean-burn engines still contain deleterious pollutants including nitrogen oxides and methane slip due to incomplete combustion [9,11–13]. Ultra-lean ($\lambda > 1.6$) combustion strategies can potentially lower in-cylinder temperatures which can further reduce heat losses, increase thermal efficiency and alleviate NOx formation, but incomplete combustion resulting in unburned methane still poses a challenge [14]. Upcoming regulations for methane emissions are likely to be even more stringent as the global warming potential (GWP) of methane is ~25 times that of CO_2 making abatement of methane emissions imperative to take advantage of the potential of lean-burn natural gas engines towards significantly mitigating greenhouse gas emissions [10,15,16].

Methane, being a stable, non-polar, saturated hydrocarbon with C-H bond dissociation energy of ~435 kJ/mol, makes catalytic activation by hydrogen abstraction and, in turn, methane oxidation challenging at low temperatures relevant to highly efficient lean-burn natural gas engine-exhaust [10,17]. The existence of high concentrations of H_2O (>10 %) in natural gas engine-exhaust, however, can inhibit methane oxidation catalysts as water competes with methane for the active sites, hindering methane activation until water desorbs from the surface of the catalysts [3,13,18,19]. Moreover, CO and NO present in the engine-exhaust will also compete for the active sites in the oxidation catalyst along with methane (CH_4) that can lead to a multi-component competitive adsorption behavior on the catalyst [20,21]. Studies have also shown

☆ This manuscript has been authored by UT-Battelle, LLC, under contract DE-AC05–00OR22725 with the US Department of Energy (DOE). The US government retains and the publisher, by accepting the article for publication, acknowledges that the US government retains a nonexclusive, paid-up, irrevocable, worldwide license to publish or reproduce the published form of this manuscript, or allow others to do so, for US government purposes. DOE will provide public access to these results of federally sponsored research in accordance with the DOE Public Access Plan (http://energy.gov/downloads/doe-public-access-plan).

* Corresponding authors.
E-mail addresses: sinhamajumds@ornl.gov (S. Sinha Majumdar), mosesmj@ornl.gov (M. Moses-DeBusk).

https://doi.org/10.1016/j.apcatb.2023.123253
Received 23 May 2023; Received in revised form 21 August 2023; Accepted 31 August 2023
Available online 4 September 2023

that carbon dioxide (CO_2), which is a major product of combustion, can strongly adsorb on basic sites active for methane activation on an oxidation catalyst leading to poisoning of the catalyst [22,23]. Preferential or stronger adsorption of one species over another within a temperature range on the surface of the catalyst can impact oxidation of the other components in the exhaust gas stream [21,24]. Therefore, a promising candidate for methane oxidation catalysis should be hydrothermally stable and demonstrate efficiency in methane conversion at low temperatures in the presence of water vapor, CO_2, CO and NO.

Superior methane combustion activity of catalysts with Pd/PdOx active sites has been widely reported [10,23,25–29]. The catalyst support has also been found to play an important role in the activity of Pd based catalysts [30–32]. The high exothermicity ($\Delta H^{\circ}_{298\ K} = -800$ kJ/mol) of methane combustion and high water vapor concentration in natural gas engine exhaust calls for a hydrothermally stable and durable catalyst to oxidize methane. The inhibition effect of water on methane oxidation for Pd-supported catalysts has been attributed to formation of less active $Pd(OH)_2$ on the surface of the catalyst [33]. Based on the affinity of the catalyst support towards water, these surface hydroxyl species can be stable beyond 250 °C, requiring higher temperatures for methane oxidation light-off under wet conditions ([34] and references therein). In addition to thermally and chemically stable supports, such as alumina and zirconia, interesting steam-resistant zeolitic materials have been recently gaining traction. Promising methane oxidation activity has been reported on tunable Pd catalysts supported on zeolites such as post-exchanged Na-ZSM-5, SSZ-39, small pore LTA, and high silica to alumina ratio (SAR) BEA and SSZ-13 materials [35–37]. Hydrophobic supports such as SSZ-13 are of particular interest due to their potential to alleviate inhibition effect of water and proven ability to maintain structural stability on exposure to engine-out exhaust.

Another component that has shown promise in improving the performance and durability of methane oxidation catalysts is Mg. Isotopic labelling studies by Rosynek et al. reported methane activation primarily via homolytic C-H bond cleavage on an MgO supported catalyst [22]. Basic sites on MgO can also aid in heterolytic splitting of C-H bond and in methane activation under lean conditions [19]. Yang and co-workers investigated PdO supported on $MgAl_2O_4$ spinel and reported better methane combustion activity due to higher dispersion of the active sites than Pd supported on an alumina reference catalyst [38]. Hu et al. studied Mg-doped Pd/ZrO_2-Al_2O_3 systems and reported Pd^{2+} stabilization with Mg on formation of $MgAl_2O_4$ spinel which helped improve dispersion and water tolerance under reaction conditions [39]. MgO addition to alumina and SSZ-13 supported catalysts can potentially reduce the acidic nature of the supports. Reducing the acidity of the support can keep Pd in the more active oxidized-state while also suppressing excessive Pd/PdOx sintering on exposure to high temperature aging conditions [40].

The aforementioned studies of methane oxidation catalysts were conducted under simple feed conditions, like most of the literature on this topic. These fundamental investigations provide valuable insights into material properties that can inform the design of methane oxidation catalysts. However, it is also important to evaluate the activity for methane oxidation under synthetic exhaust feed conditions as the constituents of the reaction mixture can have profound impacts on the catalytic activity observed. The effects of realistic exhaust mixtures open up the potential for a host of new materials for practical application under lean exhaust conditions.

In the current contribution, novel catalysts consisting of Mg incorporated into Pd supported on either SSZ-13 or alumina were synthesized. The effects of Mg addition to the Pd-based catalysts on methane oxidation activity under synthetic exhaust conditions relevant to natural gas lean-burn engines were investigated. The resulting methane oxidation catalysts were subjected to mild (500 °C) or severe (700 °C) hydrothermal aging conditions prior to activity testing. For the SSZ-13 supported catalysts, impacts of both the Pd introduction mode into the zeolite and route of Mg incorporation into the catalyst on methane conversion efficiency are presented. For gamma alumina supported catalysts, the influence of Mg on hydrothermal stability of the aged catalyst samples is discussed. The ratio of Pd:Mg was varied to optimize the synergistic effect of Mg incorporation on methane oxidation efficacy on alumina supported catalysts. Additionally, kinetic parameters such as turnover frequency, apparent activation energy and pre-exponential factors were extracted from the methane oxidation light-off curves. BET, TPR, and CO pulse chemisorption followed by TPD were used to characterize surface area, pore volume, reducibility, Pd dispersion and Pd particle size of the selected catalyst samples.

2. Experimental methods

2.1. Catalyst synthesis

2.1.1. Incipient wetness impregnation (I.W.) catalysts

The SSZ-13 zeolite used had a Si/Al ratio of 6 and was purchased from ACS materials (CAS # 1318–02–01). Elemental analysis of multiple samples confirmed the Si/Al ratio which fell within the range (5−10) listed by ACS materials. Palladium was loaded on the NH_4^+-SSZ-13 support via incipient wetness (I.W.) employing standard synthesis methods using $Pd(NO_3)_2{\cdot}2\ H_2O$ (Aldrich; CAS# 32916–07–7) precursor (step 1 in Fig. 1(a)).

Magnesium was added by I.W. to select palladium catalysts using $Mg(NO_3)_2{\cdot}6\ H_2O$ (Aldrich; CAS# 13446–18–9), except in one case in which Pd and Mg were added to the support together by co-I.W. using a mixed nitrate solution (Fig. 1). Catalysts were dried in an oven at ca. 120 °C to remove surface bound water before I.W. addition of Pd or Mg (step 2 in Fig. 1(a)). All palladium catalysts contained a palladium loading of one weight percent (1 wt%) and magnesium loadings are referenced as a molar ratio to the one weight percent Pd loading in Table 1. Pd/Al_2O_3 was purchased from Sigma Aldrich (CAS # 7440–05–3) and Mg was added via I.W. method to Pd/Al_2O_3 as described above to modify the catalysts (Fig. 1(b)).

2.1.2. Ion-exchanged (I.E.) SSZ-13 catalysts

Another set of SSZ-13 supported methane oxidation catalysts was prepared by ion-exchange (I.E.) methods. Palladium or magnesium was ion exchanged (I.E.) with the as-received NH_4^+ form of SSZ-13, following standard I.E. procedures. The SSZ-13 was added to a transparent, yellowish brown aqueous palladium nitrate solution (0.005 M) or a clear, colorless magnesium nitrate solution (0.002 M). The metal/SSZ-13 mixture was refluxed in an 80 °C oil bath for 24 h. The palladium was I.E. at 1 wt% while Mg was introduced via incipient wetness impregnation at a 1 wt% palladium molar equivalence of 0.5, 1.0 and 1.5. After cooling, the mixture was filtered, washed with deionized (DI) water, and left to air dry. The filtrate was centrifuged and filtered until all the powdered catalyst was collected by filtration. The supernatants were clear and colorless for both Pd and Mg I.E. catalysts. The air-dried powders were then dried in an oven at ca. 120 °C for 4.5 h. The Pd/SSZ-13 (I.E.) powder obtained was a light tan with a pinkish tint while the Mg/SSZ-13 (I.E.) powder was white.

2.1.3. Catalyst hydrothermal aging

Unless otherwise noted, all catalysts were hydrothermally aged in a tube furnace before testing. Table 1 describes the heat treatments and naming nomenclature for each catalyst. During aging, the powder catalysts were placed in a ceramic boat and centered in a quartz tube inside a horizontal tube furnace with a thermocouple located inside the quartz tube, in the space above the ceramic boat, for temperature control. A synthetic gas feed of oxygen and nitrogen controlled by MKS mass flow controllers at 5000 sccm was sent across the catalyst while the furnace was ramped at 2 °C/min to either 500 °C for 4 h or 700 °C for 15 h. Once the temperature reached 120 °C, water vapor was added to the gas feed using an HPLC pump (Eldex Laboratories) similar to that described by Majumdar et al. [41]. After water vapor was introduced, the feed

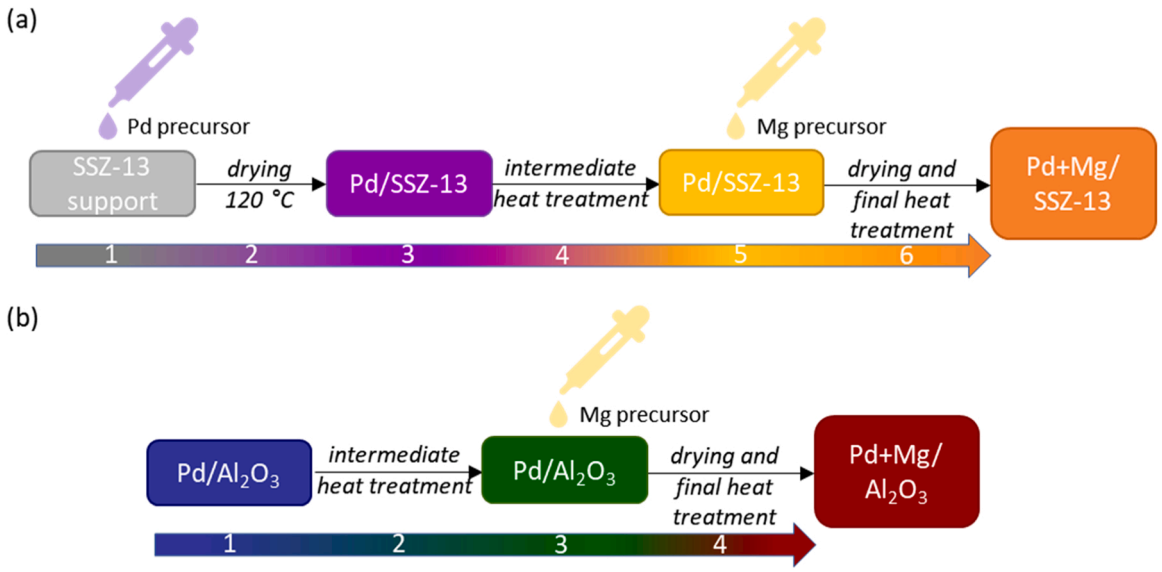

Fig. 1. Catalyst synthesis process schematic for Pd on (a) SSZ-13 (Pd introduced via I.W. or I.E.) and (b) Al_2O_3 supported catalysts. Steps (1−6) and (1−4) for (a) and (b) respectively are indicated in their corresponding arrows.

composition was 15 % O_2, 10 % H_2O with a N_2 balance. In some cases, a catalyst was subjected to two heat treatments, described in Fig. 1 and Table 1 as an intermediate and final heat treatment. For sequential bimetallic catalysts, the intermediate (Intmd.) treatment was done on the supported Pd-only catalyst while the final treatment occurred after the Mg was added to the supported Pd catalyst.

2.2. Experimental set-up details and Catalyst evaluation protocol

All catalysts were thermally or hydrothermally aged prior to catalytic evaluation, including the Pd/Al_2O_3 catalyst received from Sigma Aldrich, according to Table 1. After aging the catalysts, the catalyst powder was ground and sieved to obtain particle sizes between 150 and 250 μm to avoid channeling and elevated pressure drop effects. A 100 mg sample of catalyst was loaded into a U-tube reactor (8 mm i.d.). A K-type thermocouple was placed 0.5 cm upstream of the sample while another was positioned in the center of the powder bed to measure and record the catalyst inlet and catalyst bed temperatures, respectively. An additional thermocouple, external to the reactor tube, was used to give feedback to the temperature controller of the resistively heated furnace into which the catalyst loaded reactor tube was positioned for the light-off experiments.

Methane oxidation catalyst samples were evaluated under full synthetic exhaust-gas composition as per industry guidelines delineated in the U.S. Drive low-temperature oxidation catalyst test protocol [42]. A bank of mass flow controllers (MKS instruments and Teledyne Hastings) was used to simulate the full synthetic exhaust conditions under which the methane oxidation experiments were conducted. A stream of Argon (Ar) was saturated by flowing it through a water bubbler immersed in a recirculating bath set to 62 °C to introduce 12 % H_2O in a preheated gas feed containing 9 % O_2, 6 % CO_2, 3000 ppm CH_4, 2000 ppm CO, 500 ppm NO during the light-off experiments. The gas lines in the reactor system were maintained at ~200 °C to eliminate condensation of water or adsorption of reactants in the lines. The total flow rate to the reactor was 333 sccm resulting in a catalyst-mass-normalized flow of 200 L/g-h. Gas compositions of the reactor feed and product streams were measured using a MKS Instruments Multigas 2030HS FTIR spectrometer operated at 1 Hz. To improve the response times within the FTIR, the gas stream being measured was diluted with 666 sccm Ar before being analyzed by the FTIR.

The reaction profile used for methane light-off experiments is shown in Fig. 2 [42]. The pre-treatment and reaction feed conditions are tabulated in Table 2. A catalyst sample was first pretreated under oxidizing conditions at 600 °C for 20 min, then cooled under the same conditions to 300 °C at which point the remaining constituents of the synthetic exhaust-gas mixture were switched on. After stabilization of the catalyst temperature and reactant flows, the catalyst inlet temperature was ramped at 5 °C/min to 600 °C. From the methane oxidation light-off curve obtained during the experiment, the catalyst inlet temperatures at which 50 % (T_{50}) and 90 % conversion (T_{90}) of methane were achieved are used to compare the methane oxidation efficiency of the catalyst samples. The light-off experiments were repeated three times for two alumina supported samples (with and without Mg) shown in Fig. S1.

2.3. Catalyst characterization

2.3.1. BET surface area and BJH pore volume analysis

N_2 adsorption-desorption isotherms were collected at 77 K on selected catalysts using a Quantachrome 1-C analyzer for surface area and pore volume analysis. Prior to N_2 physisorption, 100 mg of each catalyst sample was outgassed at 150 °C for 4 h. Specific surface area (S.S.A.) of the catalysts were calculated using a multipoint BET (Brunauer-Emmett-Teller) method while pore volume was analyzed using BJH (Barrett-Joyner-Halenda) for the mesoporous samples and NLDFT (Non-local Density Functional Theory) for the microporous samples.

2.3.2. H_2 temperature-programmed reduction (TPR)

H_2-TPR was carried out on selected catalysts in a Micromeritics AutoChem II 2920 equipped with a TCD detector. Each catalyst (100 mg) was pre-treated under 30 sccm of 10 % O_2/Ar at 600 °C and cooled to − 40 °C using the Micromeritics Cryo-cooler under oxidizing conditions. The catalyst was then flushed with 30 sccm Ar followed by introduction of 30 sccm 2 % H_2/Ar into the reactor. The TPR was performed by heating the reactor to 600 °C at a ramp rate of 10 °C/min under 2 % H_2/Ar.

2.3.3. CO-pulse chemisorption and temperature-programmed desorption (TPD)

Selected catalysts were subjected to CO-pulses using an AutoChem II 2920 Micromeritics instrument equipped with a TCD detector to gain insights into the dispersion and particle size of Pd on the catalysts. A

Table 1
Methane oxidation catalysts synthesized and catalyst light-off temperature summary after different hydrothermal heat treatments.

Catalysts Synthesized	Mg Addition[a]	Pd: Mg	Heat Treatment (°C) (700 °C-15 h /500 °C-4 h)		Total Aging (h)	T_{50} | T_{90} (°C)
			Intmd.	Final		
Pd (I.E.)/SSZ-13 supported Catalysts						
Pd(I.E.)/SSZ-13 HTA 500 C	-	1:0	-	500	4	471 | > 600
Pd(I.E.)/SSZ-13 cal. 500 C-HTA 700 C	-	1:0	500[b]	700	15	484 | > 600
Pd(I.E.)/SSZ-13 HTA 700 C	-	1:0	-	700	15	461 | > 600
Pd(I.E.)+Mg/ SSZ-13 HTA 500 C	Seq. I.W.	1:1	700	500	19	> 600
Pd (I.W.)/SSZ-13 supported Catalysts						
Pd(I.W.)/SSZ-13 HTA 500 C	-	1:0	-	500	4	515 | 600
Pd(I.W.)+Mg/ SSZ-13 HTA 500 C	Seq. I.W.	1:1	500	500	8	499 | 557
Pd(I.W.)_Mg/ SSZ-13 HTA 500 C	Seq. I.W.	1:1	120[c]	500	4	505 | 559
PdMg(co-I.W.)/ SSZ-13 HTA 500 C	Co-I.W.	1:1	-	500	4	576 | > 600
Sigma Aldrich (Pd/Al_2O_3)						
Pd/Al_2O_3 (Fresh)	-	1:0	-	-	-	404 | 456
Pd/Al_2O_3 HTA 500 C	-	1:0	-	500	4	404 | 433
Pd/Al_2O_3 HTA 700 C	-	1:0	-	700	15	411 | 466
$Pd+Mg/Al_2O_3$ HTA 500 C	Seq. I.W.	1:1	500	500	8	409 | 450
1.0 Pd+ 0.5Mg/ Al_2O_3 HTA 700 C	Seq. I.W.	1:0.5	700	700	30	438 | 574
1.0 Pd+ 1.0Mg/ Al_2O_3 HTA 700 C	Seq. I.W.	1:1	700	700	30	406 | 454
1.0 Pd+ 1.5Mg/ Al_2O_3 HTA 700 C	Seq. I.W.	1:1.5	700	700	30	411 | 461

[a] Seq. refers to the sequential I.W. addition of Mg
[b] calcined under air
[c] dried under air

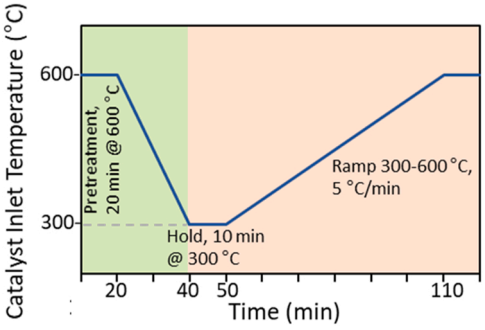

Fig. 2. Reaction profile for methane oxidation catalyst evaluation with pre-treatment (green) and light-off (orange) composition indicated in color. Gas compositions listed in Table 2.

Table 2
Reactant gas composition (in balance N_2) for catalyst evaluation.

Step	$[O_2]$ %	$[CO_2]$ %	$[H_2O]$ %	[NO] ppm	[CO] ppm	$[CH_4]$ ppm
Pretreatment	9	6	12	-	-	-
Light-off	9	6	12	500	2000	3000

Pfeiffer OmniStar quadrupole mass spectrometer was connected downstream of the AutoChem II for additional analysis of the effluent gas stream from the reactor tube. A 50 mg catalyst sample was loaded into a U-tube reactor and pre-treated under 50 sccm of 10 % O_2/Ar at 600 °C to oxidize the catalyst and remove any adsorbed impurities. The catalyst was then cooled to 450 °C, flushed with Ar, and reduced under 50 sccm of 10 % H_2/Ar for 60 min. The catalyst was further cooled to 150 °C in the reducing environment. The reduced catalyst was flushed with 50 sccm Ar at 150 °C to remove any adsorbed H_2, then finally cooled to 40 °C to perform CO-pulse chemisorption. A loop of 0.56 mL volume was filled with 1 % CO/Ar and Ar flow of 50 sccm was used to inject the loop volume into the U-tube reactor. Using the loop injection, CO was pulsed onto the catalyst until saturation (indicated by constant pulse area). After the catalyst surface was saturated with CO, temperature-programmed desorption was performed under 50 sccm Ar from 40 °C to 500 °C at a ramp rate of 5 °C/min to characterize the Pd sites based on their CO binding strength.

3. Results and discussion

3.1. Catalyst characterization and methane oxidation activity measurements

The specific surface area and pore volume of selected methane oxidation catalysts are summarized in Table S1 (supplementary information). The SSZ-13 supported samples exhibited Type I isotherms (under N_2 physisorption) characteristic of microporous samples with large surface areas being attributed to the microporous region [43]. A major contribution to the pore volume of these catalysts is from pores in the micropore size range (<12 Å). The alumina supported samples, on the other hand, displayed Type IV(a) BET isotherms (C>>10) with a broad pore size distribution in the mesopore range (16–180 Å) and maximum pore diameters within 65–85 Å [43]. Furthermore, on comparing the mildly aged (500 °C, 4 h) vs. severely aged (700 °C, 15 h) Pd catalyst, a decrease in specific surface area from 103 m^2/g to 91 m^2/g was observed. Incorporation of Mg to the respective Pd catalysts does not significantly impact the specific surface area or pore volume of the resulting catalysts even after further aging at 500 °C for 8 h or at 700 °C for 30 h. In the following sections, further characterization and methane oxidation catalyst activity has been evaluated to gain insights into the impact of Mg addition to Pd based methane oxidation catalysts.

3.1.1. SSZ-13 supported catalyst characterization

3.1.1.1. CO-pulse chemisorption on selected SSZ-13 supported MOCs. Based on the amount of CO adsorbed, Pd dispersion and particle sizes (assuming hemispherical Pd particles) were estimated for selected methane oxidation catalysts using CO-pulse chemisorption and are tabulated in Table 3. The reduction temperature (450 °C) prior to CO-pulses was determined based on H_2-TPR profiles (discussed in Section 3.1.1.3) and were not expected to have a significant impact on the dispersion of the active sites on the catalysts. A Pd loading of 1 wt% and a Pd:CO ratio of 1:1 were assumed for each of the dispersion calculations [40].

In the case of SSZ-13 supported catalysts, high Pd dispersion (Table 3) was observed in Pd(I.E.)/SSZ-13. Hydrogen treatment prior to CO pulses can reduce ion-exchanged Pd cations (Pd^{2+}) into metallic Pd particles (Pd^0) which in turn can contribute to elevated adsorption of CO

Table 3
CO-pulsed chemisorption on selected SSZ-13 supported methane oxidation catalysts.

Samples[a]	CO Consumed (μmol/g)	Dispersion (%)	Particle Size (nm)	L_1/L_2[b] Ratio
Pd(I.E.)/SSZ-13 HTA 700 C	4.1	85	1.1	0.5
Pd(I.E.) +Mg/ SSZ-13 HTA 500 C	3.7	77	1.2	0.6
Pd(I.W.)/SSZ-13 HTA 500 C	2.1	45	2.0	0.5
Pd(I.W.) +Mg/ SSZ-13 HTA 500 C	1.7	35	2.6	0.6

[a] Pd:Mg is 1:1 molar ratio for all bimetallic samples, Mg added sequentially via I.W.
[b] $L_1/L_2 \equiv$ Pd(1 0 0)/Pd(1 1 1) estimated from CO TPD.

[44]. Thus, the high Pd dispersion in the I.E. samples suggested effective ion-exchange was achieved resulting in atomically dispersed Pd^{2+} cations inside the zeolite cages, with minimal formation of bulk PdOx particles in the synthesized catalyst. Interestingly, the addition of magnesium and subsequent second hydrothermal exposure (500 °C/4 h) in the synthesis of Pd(I.E.)+Mg/SSZ-13 reduced the Pd dispersion by 8 % but had little impact on the particle size compared to the Pd(I.E.) only catalyst.

On the other hand, Pd addition by incipient wetness resulted in a significant drop in Pd dispersion within the SSZ-13 support, Pd (I.W.)/SSZ-13, indicative of an increased formation of bulk PdOx particles compared to Pd^{2+}. Addition of Mg to Pd(I.W.)/SSZ-13 followed by the subsequent second hydrothermal aging exposure (500 °C/4 h), resulted in reduction of the Pd dispersion from 45 % to 35 % which corresponded to an increase in the Pd/PdOx particle size from 2.0 to 2.6 nm. The increasing Pd particle size with decreasing metal dispersion is consistent with the assumption of hemispherical Pd particles. As slight sintering of the active Pd/PdOx sites has been shown to be beneficial for methane oxidation under lean conditions, the I.W. samples are expected to exhibit better methane oxidation activity than the I.E. samples [45,46].

3.1.1.2. CO and CO_2 temperature-programmed desorption (TPD). CO-pulse chemisorption of selected catalysts was followed by temperature-programmed desorption (TPD) under Ar to gain valuable information about the type of Pd active sites based on their CO binding strength. The CO ($m/z = 28$) and CO_2 ($m/z = 44$) signals obtained from the mass spectrometer during TPD from 40 °C to 500 °C after CO adsorption is depicted in Fig. 3(a) and (b). The SSZ-13 samples displayed three distinct CO desorption features (Fig. 3(a)): a low temperature peak between 90 °C and 150 °C (L_1), a mid-temperature peak centered ~190 °C (L′), and a high temperature peak in the 300–350 °C range (L_2). As CO binding strength depends on the type of adsorption site, the appearance of multiple CO desorption peaks suggests the presence of three distinct adsorption sites for CO. Stara et al. and Monteiro et al. attributed the low temperature feature (L_1) to linearly bound CO on Pd (1 0 0) faces and the high temperature peak (L_2) to linearly bound CO on Pd (1 1 1) faces [47,48]. Methane oxidation occurs via the Mars-van Krevelen mechanism which is favored on Pd (1 0 0) over the denser, hexagonal-close packed, and sterically constrained Pd (1 1 1) crystal plane [49,50]. Therefore, the relative ratio of the two linearly bound CO desorption peaks (L_1/L_2) corresponding to the Pd (1 0 0)/Pd (1 1 1) ratio (Table 3) can provide interesting insights into methane oxidation efficiencies observed for the catalyst samples investigated in this study.

In general, the L_1/L_2 ratio for all the SSZ-13 catalysts studied were less than 1, indicating that there were more Pd (1 1 1) sites than Pd (1 0 0) within the catalysts. Oxygen exchange and formation of surface oxides, which are beneficial for methane oxidation via a redox mechanism, are less facile on the sterically constrained and compact Pd (1 1 1) facets and may negatively impact methane oxidation activity on the SSZ-13 supported catalysts [49]. Furthermore, the mode of Pd addition to SSZ-13 and thermal aging history had little impact on the L_1/L_2 and only a marginal increase after addition of Mg was observed.

The intermediate CO desorption peak (L′), possibly arises from CO adsorbed on Pd^0 particles formed by reduction of Pd^{2+} within the zeolite cage during hydrogen exposure preceding CO chemisorption. Therefore, the L′ peak indicates the presence of Pd^{2+} catalyst sites compared to Pd particles indicated by the L_1 and L_2 peaks. The L′ CO feature had the highest contribution in the Pd(I.E.)/SSZ-13 catalyst which based on dispersion measurement suggested it also contained the most I.E. Pd^{2+} species. Mg incorporation led to a drop in L′ sites on Pd(I.E.)+Mg/SSZ-13 suggesting fewer Pd^{2+} sites. This may have resulted from conversion of the Pd^{2+} to Pd/PdOx particles during the additional hydrothermal exposure after Mg addition. It can also be envisioned that further Pd/PdOx particle agglomeration was diminished in Pd(I.E.)+Mg/SSZ-13 catalyst on aging due to MgO blocking a portion of the zeolite cages. Blockage of the cages may have kept the Pd/PdOx particles segregated within the cage resulting in particle sizes of ~ 1 nm similar to that in reduced Pd (I.E.)/SSZ-13 which have been reported to be less active for methane oxidation [45,51].

While I.W. Pd introduction to SSZ-13 resulted in a lower contribution of the L′ peak to the overall CO desorption spectra compared to that introduced by I.E, it was still a notable contribution that suggested that a fraction of the Pd in Pd(I.W)/SSZ-13 was in the Pd^{+2} state. The elevated Pd dispersion for Pd(I.W)/SSZ-13 estimated using CO-pulse chemisorption also supports the presence of cationic Pd^{2+} in Pd(I.W)/SSZ-13. However, only half the amount of CO was consumed on Pd(I.W)/SSZ-13 compared to Pd(I.E.)/SSZ-13 during the chemisorption study (Table 3) further indicating that lower ion-exchange efficiency was achieved for Pd(I.W)/SSZ-13 as intended by the I.W. synthesis approach. Interestingly, addition of Mg to Pd(I.W)/SSZ-13 demonstrated a further reduction in L′ CO desorption peak suggesting limited Pd^{2+} sites. The increased particle size, lower dispersion and reduced L′ peak contribution all indicate that the Pd(I.W)+Mg/SSZ-13 catalyst had the greatest fraction of Pd as Pd/PdOx particles among the SSZ-13 supported catalysts studied. As Pd/PdOx particles aid methane oxidation, the Pd(I.W)+Mg/SSZ-13 catalyst was expected to have higher methane conversion than the other zeolite supported samples investigated in this study.

Additionally, for all the samples investigated in this study, simultaneous evolution of CO_2 was observed with CO desorption as depicted in Fig. 3(b). Formation of CO_2 is mainly ascribed to disproportionation of CO [$2CO \rightarrow CO_2 + C$] on the tetra-coordinated Pd (1 0 0) facets which are favorable for lean CH_4 oxidation. Water gas shift reaction (WGS) of bridge-bonded CO on Pd with residual moisture is another pathway to CO_2 formation [48,52]. However, absence of bridge-bonded CO and corresponding CO_2 desorption peaks due to WGS reaction typically arising beyond 400 °C in the respective TPD profiles (Fig. 3), suggest that CO disproportionation occurs primarily on small Pd/PdOx particles and is in good agreement with particle sizes estimated from CO-pulse experiments shown in Table 3.

3.1.1.3. H_2 temperature programmed reduction (TPR). To gain insights into the reducibility of the Pd/PdOx active sites, H_2 TPR characterization was done on selected SSZ-13 supported catalyst samples. The H_2 consumption TPR profiles are displayed in Fig. 3(c) and (d). Prior to exposing the Pd-containing catalyst samples to H_2, a controlled H_2-TPR experiment was conducted on the bare NH_4^+-SSZ-13 support to avoid overestimating H_2 consumption in the low temperature range in which PdOx aggregates are typically expected to reduce. The broad peak centered at ~ − 20 °C in the TPR profile of the bare NH_4^+-SSZ-13 support (likely converted to H-SSZ-13 on pretreatment prior to TPR) was attributed based on the literature to desorption of Ar from the zeolite support and was observed in the reduction profile for all the SSZ-13

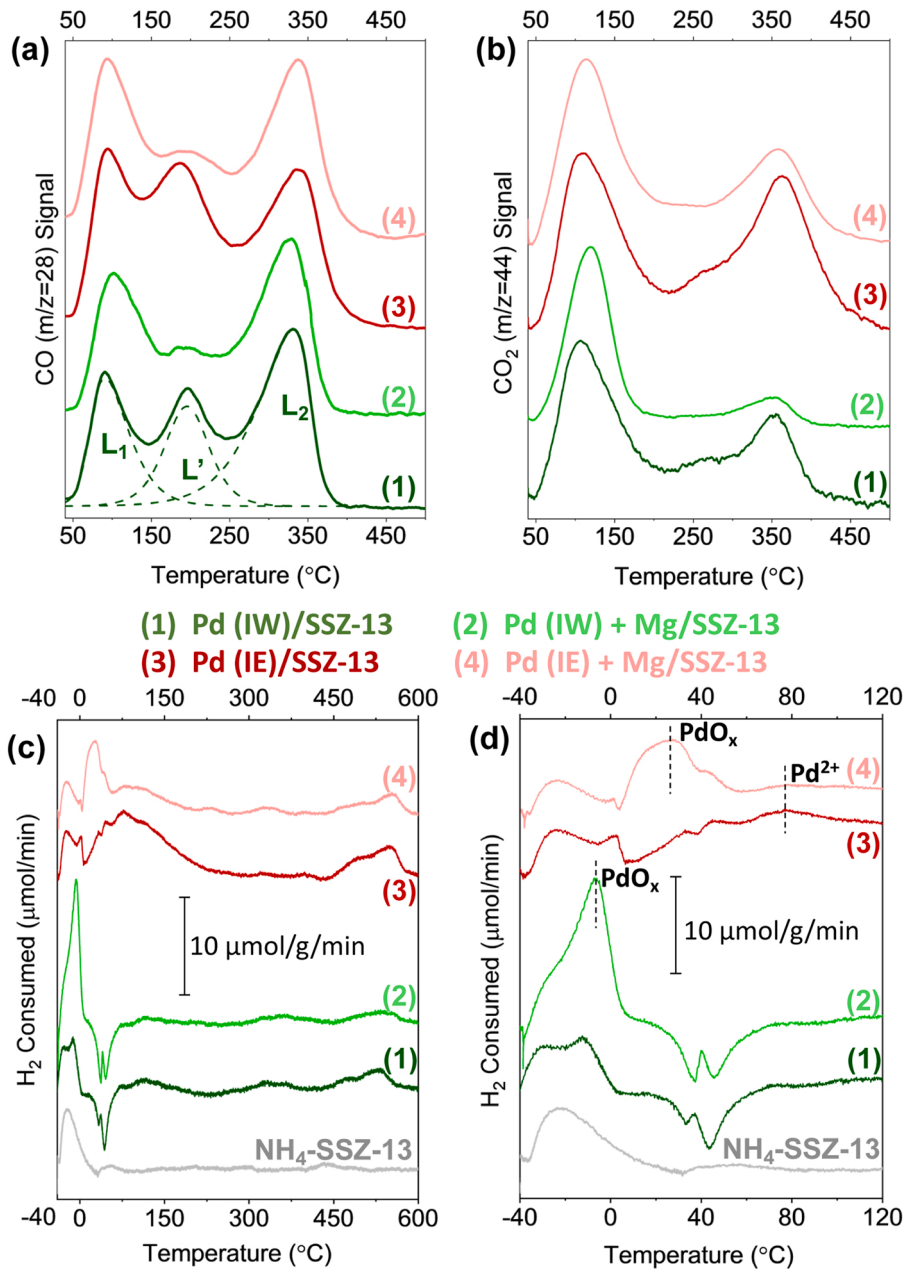

Fig. 3. (a) CO (*m/z* 28) and (b) CO_2 (*m/z* 44) during temperature-programmed desorption following CO-pulse chemisorption where dotted green lines show peaks L_1, L', and L_2 obtained by deconvolution of the CO TPD profile for the catalyst; and (c) H_2-TPR profiles from − 40 °C to 600 °C with (d) Zoom in of low temperature TPR peaks between − 40 °C to 120 °C for the SSZ-13 samples.

supported catalysts displayed in Fig. 3(c) and (d) [53].

The H_2-TPR profile of the Pd(I.E.)/SSZ-13 catalyst exhibited low intensity features corresponding to low temperature reduction of PdOx species. Typically, under the H_2 partial pressure used during these TPR experiments, once PdOx is reduced to Pd by H_2 at low temperatures, H_2 could then adsorb onto Pd to form palladium hydride (PdH_x) at room temperature. Ramping the catalyst temperature beyond room temperature would then lead to decomposition of PdH_x species with evolution of H_2 from the sample and may be observed as negative H_2 consumption features in the TPR profiles. For the Pd(I.E.)/SSZ-13, the peaks corresponding to decomposition of palladium hydride (PdH_x) are also low in intensity as expected for ion-exchanged samples. The intense broad peaks centered ~80 °C in the TPR profile are typically attributed to Pd^{2+} cations in the zeolite cage and further confirmed high Pd ion-exchange efficiency for the catalyst [44,53]. Additionally, high temperature reduction features at 500 °C and 550 °C (Fig. 3(c)) arising from stable Pd^{2+} cations were also observed for Pd(I.E.)/SSZ-13.

Mg addition via incipient wetness impregnation to Pd(I.E.)/SSZ-13 resulted in a broad PdOx reduction peak at 20 °C which is characteristic of smaller PdOx particles. Evidence of these smaller PdOx particles along with lower intensity features associated with Pd^{2+} cations in the cages and ion-exchanged Pd^{2+} in Pd(I.E.)+Mg/SSZ-13, suggest either a loss of cationic Pd^{2+} due to additional hydrothermal aging at 500 °C or a decrease in accessibility of the Pd^{2+} cations due to blockage of the cages with MgO. With the presence of PdOx particles, usually a corresponding intense negative PdH_x peak is expected in the TPR profile. However, PdH_x decomposition features are curiously absent in the TPR profile for Pd(I.E.)+Mg/SSZ-13 suggesting that the PdOx reduction peak observed at 20 °C is associated with small PdOx particles possibly interacting strongly with MgO in the zeolite cage resulting in a shift to higher

reduction temperature. The absence of a reduction peak corresponding to large PdOx clusters at lower temperature likely shows that the formation of large PdOx on hydrothermal aging of Pd(I.E.)+Mg/SSZ-13 at 500 °C was hindered. This observation could be ascribed to isolation of the Pd species within the zeolite cage due to MgO blocking the pores resulting in overstabilization of the small PdOx particles formed in the cage by strong interaction with Mg [40]. Additionally, the electropositive nature of Mg can potentially destabilize hydrides formed on small PdOx particles strongly interacting with MgO [54].

A peak at − 11 °C associated with reduction of large PdOx aggregates was seen for the Pd(I.W.)/SSZ-13 and increased with slight shift in temperature into a sharp feature after Mg incorporation, Pd(I.W.)+Mg/SSZ-13. The sharp PdOx reduction feature observed signifies displacement of more Pd^{2+} from the zeolite cage to form PdOx after addition of Mg and subsequent hydrothermal aging at 500 °C. Intermingling of Pd with Mg during redispersion of PdOx on SSZ-13 during aging likely alters the interaction of PdOx with the support and stabilizes the particles on SSZ-13, as was suggested by the shift in reduction temperature to − 6 °C. The strong reduction peak at − 6 °C suggests a significant portion of the Pd species were in PdOx form with a comparatively narrow Pd/PdOx particle size distribution. In contrast to the I.E samples, PdH_x decomposition peaks were observed for both I.W. samples emphasizing the formation of larger PdOx particles in the latter samples. Furthermore, reduction features assigned to Pd^{2+} cations inside the zeolite cages were observed at low intensity for both I.W. samples at ~ 115 °C and at 540 °C indicative of the reduced ion-exchange efficiency when the I.W. method was used for catalyst synthesis.

3.1.2. *Evaluation of CH_4 oxidation activity under simulated-engine exhaust conditions*

3.1.2.1. Effect of introduction method of Pd to SSZ-13. The mode of introduction of Pd into a zeolite support such as SSZ-13 has been found to significantly impact the state of the Pd in the catalyst which, in turn, influences the performance of the catalyst [55,56]. Pd was first introduced to SSZ-13 via ion-exchange method (Pd (I.E.)/SSZ-13) to facilitate high Pd dispersion in the zeolite support [57]. Most catalyst synthesis procedures include a calcination treatment step to stabilize and activate the final form of the catalyst. Exposure of the Pd/SSZ-13 to high temperature under dry air, however, could lead to sintering of Pd resulting in loss of catalytic activity [58,59]. On the other hand, hydrothermal aging of these materials has been found to promote Pd dispersion in the ion-exchange sites of the zeolite [60,61]. Thus, prior to evaluating the catalyst for methane oxidation activity in our study, two modes of hydrothermal aging were adopted: (i) mild aging at 500 °C for 4 h (HTA 500 C) and (ii) severe aging at 700 °C for 15 h (HTA 700 C). For comparison with traditional oxidation catalysts, an additional sample was evaluated which was calcined under air at 500 °C followed by severe aging at 700 °C for 15 h (calcined@500 C-HTA 700 C).

After hydrothermal aging, the catalytic oxidation activity of the Pd(I.E.)/SSZ-13 catalyst samples were evaluated under full synthetic exhaust conditions relevant to lean natural-gas fueled engines (Table 2). Complete oxidation of CO by 175 °C (not shown for brevity) was observed for all three catalyst samples. Under lean conditions, reducing NO to N_2 is challenging. Notably, we did not observe any N_2O formation for the Pd(I.E.)/SSZ-13 samples. As this study was focused on the catalytic activity for low temperature methane oxidation, the catalysts were compared based on their light-off behavior for methane as shown in Fig. 4.

The methane oxidation performance of the catalyst samples were quantified based on T_{50} and T_{90} results (temperature at which 50 % and 90 % methane is oxidized on the catalyst, respectively) and are displayed in the Fig. 4 bar graph. The T_{50} after mild hydrothermal aging of Pd(I.E.)/SSZ-13 (HTA 500 C) was 471 °C while severe hydrothermal aging (HTA 700 C) decreased the T_{50} to 461 °C. However, in the case of the sample with the dry calcination step before hydrothermal aging (calcined@500 C-HTA 700 C), the T_{50} increased to 484 °C.

While the active site for methane oxidation under lean conditions has been debated in the past, the general consensus is that Pd/PdOx particles in the range of 2–7 nm (combination of Pd oxidation states) are highly active for methane oxidation under lean conditions for Pd-supported catalysts [64]. Li et al. and Maeda et al. each proposed that highly dispersed Pd^{2+} in zeolites such as ZSM-5 could also be active for methane combustion due to the oxygen-exchange capability of the zeolite support [57,62]. Recently, Friberg et al. and Petrov et al., on the other hand, reported lower methane oxidation activity for Pd^{2+} cations ion-exchanged into zeolites and agreed that PdOx particles were indeed more active for methane oxidation under lean conditions [35–37].

Ryou et al. found ion-exchanging Pd into SSZ-13 by conventional methods challenging due to the small pore-size of the zeolite and observed that hydrothermal aging at temperatures higher than 650 °C facilitated the mobility of small PdO particles into the zeolite and enabled its transformation into Pd^{2+} cations [60,63]. The lower hydrothermal aging temperature (500 °C) of the Pd(I.E.)/SSZ-13 (HTA 500 C) sample may have led to ineffective dispersion of Pd species [44,63]. CO pulse chemisorption experiments revealed high ion-exchange efficiency in Pd(I.E.)/SSZ-13 (HTA 700 C) indicating that most of the

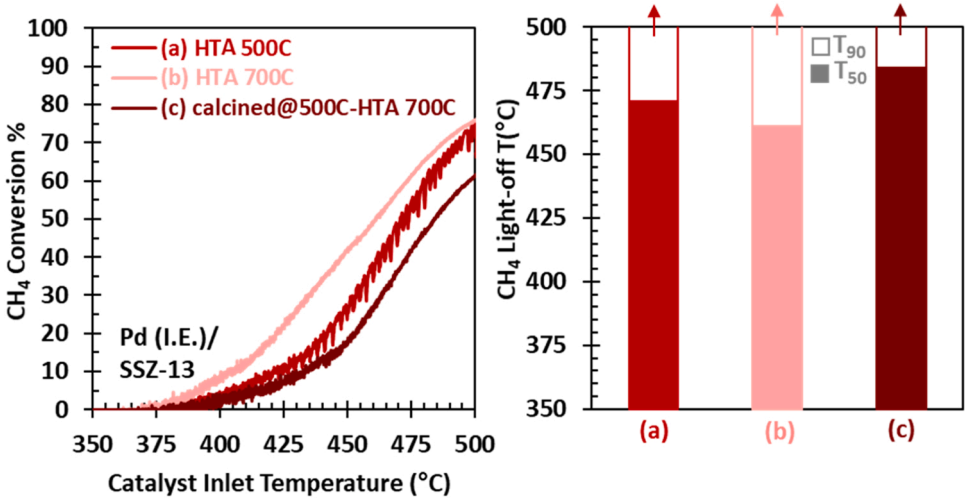

Fig. 4. Comparison of CH_4 conversion on Pd(I.E.)/SSZ-13 after (a) mild hydrothermal aging (500 °C/4 h), (b) severe hydrothermal aging (700 °C/15 h) or (c) dry air calcination (500 °C/4 h) followed by a severe hydrothermal aging. T_{50} and T_{90} are compared in the bar graph for (a), (b) and (c) where arrows indicate T_{90} was not reached by 500 °C. Feed Conditions: 9 % O_2, 6 % CO_2, 12 % H_2O, 2000 ppm CO, 500 ppm NO, 3000 ppm CH_4.

Pd is likely in Pd^{2+} cationic form in the zeolite cage. H_2 TPR experiments also indicated the presence of small PdO particles in the severely aged sample which may aid early combustion of CH_4 thus lowering the T_{50} observed for methane oxidation for the Pd(I.E.)/SSZ-13 (HTA 700 C) sample [64]. On the other hand, with dry calcination of the Pd(I.E.)/SSZ-13 catalyst under air at 500 °C, the consumption of the paired Brønsted acid sites in the zeolite may cause the Pd species within the SSZ-13 cages to agglomerate resulting in the formation of encapsulated PdO particles which could explain the higher T_{50} observed in the case of the calcined catalyst [65]. Regardless of treatment, none of the Pd(I.E.)/SSZ-13 samples reached 90 % conversion for methane oxidation under the synthetic exhaust conditions, indicated by the arrows in the Fig. 4 bar graph.

To increase the methane combustion active Pd/PdOx sites, Pd was introduced to SSZ-13 using incipient wetness impregnation (Pd (I.W.)/SSZ-13). The resulting catalyst was hydrothermally aged at 500 °C (HTA 500 C) and evaluated for its methane oxidation efficacy. On comparing the T_{50} of the I.W. catalyst (Fig. 5(c)) with the hydrothermally-aged (HTA 500 C) Pd ion-exchanged into SSZ-13 (I.E.) in Fig. 5(a), we observe an elevated T_{50} in the case of I.W. catalyst (ΔT_{50} ~44 °C). However, methane conversion of 90 % was achieved by 600 °C (T_{90}) when Pd was introduced to SSZ-13 via I.W. method unlike the I.E. catalyst which did not achieve 90 % conversion of methane within the 600 °C temperature range investigated. H_2-TPR experiments discussed earlier indicated that when Pd was introduced to SSZ-13 via I.W., PdOx particles were likely formed on the SSZ-13 support. The lower T_{90} of the Pd(I.W.)/SSZ-13 catalyst may be due to the presence of Pd/PdOx particles on SSZ-13 which have been reported to have promising activity for methane oxidation [64,66–68].

3.1.2.2. Effect of Mg addition to Pd/SSZ-13. Addition of Mg to oxidation catalysts has been reported to aid in hydrogen abstraction from methane, which is considered the rate limiting step in methane oxidation under dry conditions, along with improving the thermal stability of the resulting catalyst [39,69–74]. To understand the impact of Mg on the SSZ-13 methane oxidation catalysts, Mg was introduced via incipient wetness impregnation method to Pd(I.E.)/SSZ-13 HTA 700 C and Pd(I.W.)/SSZ-13 HTA 500 C followed by additional hydrothermal aging at 500 °C (HTA 500 C). After Mg incorporation, the methane light-off temperatures of Pd (I.E.)+Mg/SSZ-13 and Pd (I.W.)+Mg/SSZ-13 were measured from 300 °C to 600 °C under synthetic exhaust conditions and are included in Fig. 5.

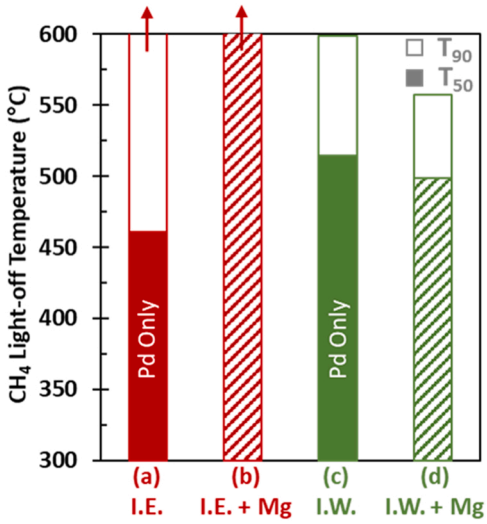

Fig. 5. Comparison of T_{50} (solid or patterned fill) and T_{90} (void fill) CH_4 light-off temperatures for Pd(I.E.) and Pd(I.W.) SSZ-13 catalyst before and after sequential Mg addition, HTA 500 C treatments after Pd and Mg additions: (a) Pd(I.E.)/SSZ-13, (b) Pd+Mg(I.E.)/SSZ-13, (c) Pd(I.W.)/SSZ-13 and (d) Pd+Mg (I.W.)/SSZ-13 catalysts. Arrows indicate T_{90} was not reached by 600 °C. Feed Conditions: 9 % O_2, 6 % CO_2, 12 % H_2O, 2000 ppm CO, 500 ppm NO, 3000 ppm CH_4.

Comparison between Fig. 5(a) and (b) shows that incorporation of Mg into Pd(I.E.)/SSZ-13, pushed the T_{50} temperature higher than 600 °C. As Mg was added to Pd(I.E.)/SSZ-13 via incipient wetness impregnation method, the loss in methane oxidation activity might be ascribed to the formation of MgO particles on SSZ-13 after aging which could in turn cause pore blockage and prevent access to the small Pd/PdOx sites within the zeolite framework. Additionally, CO pulse chemisorption and H_2-TPR indicated the presence of Pd^{2+} cations along with small (~1.2 nm), less reducible Pd/PdOx particles, providing a possible explanation for the low methane oxidation activity exhibited by Pd(I.E.)+Mg/SSZ-13 sample. The presence of Pd/PdOx particles in the 2–7 nm size range have been shown to be optimum for methane oxidation activity [46,64,75]. Furthermore, minimal methane oxidation was observed over an Mg(I.E.)/SSZ-13 catalyst (not shown) which indicated that Mg by itself did not exhibit significant methane oxidation activity.

The beneficial effect of addition of Mg to Pd(I.W.)/SSZ-13 on methane conversion demonstrated in Fig. 5(c) and (d) where both T_{50} and T_{90} for the Pd(I.W.)+Mg/SSZ-13 catalysts were lower than the corresponding Mg free catalyst, Pd(I.W.)/SSZ-13 (ΔT_{50} ~16 °C and ΔT_{90} ~43 °C). The superior methane conversion after Mg addition to the Pd(I.W.) catalyst may have resulted due to a synergistic effect resulting from the proximity between the Pd and Mg particles on SSZ-13 after aging the sample. Close proximity of the particles might allow Mg to aid in hydrogen abstraction from methane at lower temperatures followed by a subsequent oxidation by the Pd/PdOx particles [22,40]. Furthermore, the increase in Pd/PdOx particle size to 2.6 nm as estimated using CO pulse chemisorption may also be beneficial to lowering the T_{90} for methane oxidation. While small PdO particles (~1–2 nm) can participate in combustion of CH_4, it is widely accepted that medium sized Pd/PdOx (~2–7 nm) sites are likely optimum for methane oxidation under lean conditions [64,76,77]. For all the samples, complete CO oxidation was observed below 300 °C.

To further understand the effect of the route of Mg addition to Pd (I.W.)/SSZ-13 on methane oxidation efficiency of the resulting catalyst, three modes of Mg incorporation were investigated. The Mg was either sequentially added via I.W. to Pd (I.W.)/SSZ-13 HTA 500 C, dried Pd(I.W.)/SSZ-13 (at 120 °C) or co-impregnated by I.W. with Pd on the SSZ-13 support. All three catalysts were then hydrothermally aged at 500 °C (HTA 500 C) before being evaluated for their methane oxidation performance. Sequential incorporation of Mg to either Pd (I.W.)/SSZ-13 HTA 500 C or dried Pd (I.W.)/SSZ-13 results in comparable T_{50} and T_{90} for methane conversion as depicted in Fig. 6(b) and (c) with both Mg-containing catalysts demonstrating higher methane oxidation activity than the Pd-only (I.W.) sample as observed in Fig. 6(a). On the other hand, a significantly higher T_{50} (576 °C) and T_{90} (>600 °C) was observed in the case of PdMg (co-I.W.)/SSZ-13 HTA 500 C catalyst shown in Fig. 6(d) compared to the Pd only and the sequential Mg incorporated samples. Co-I.W. of Pd and Mg on SSZ-13 may have led to one species preferentially being impregnated on SSZ-13 depending on the precipitation characteristics of the precursors used, disrupting the synergistic effect between Pd and Mg due to altered electronic environments. Further studies are required to fully understand the negative effect of co-I.W. preparation.

3.1.3. Al_2O_3 supported catalyst characterization

3.1.3.1. CO-pulse chemisorption on selected Al_2O_3 -supported MOCs. The Pd dispersion and particle size of the Al_2O_3 supported MOCs were estimated using CO pulse chemisorption (Table 4) assuming hemispherical Pd particles and Pd:CO ratio of 1:1. The catalyst samples were reduced

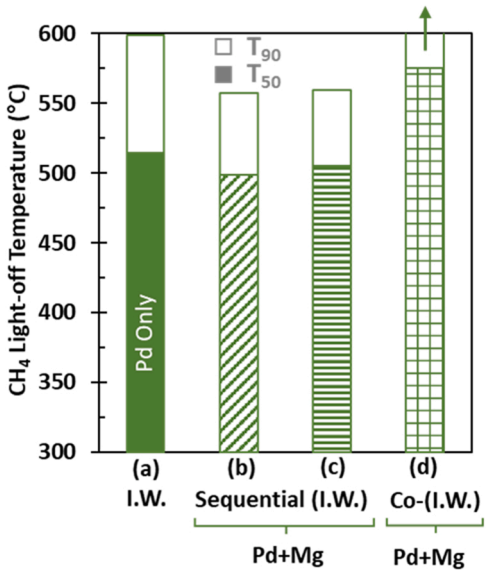

Fig. 6. Comparison of T_{50} (solid or patterned fill) and T_{90} (void fill) CH_4 light-off temperatures for (a) Pd (I.W.)/SSZ-13 HTA 500 C (solid fill), (b) sequentially added Mg to Pd (I.W.)/SSZ-13 HTA 500 C (diagonal fill), (c) sequentially added Mg to dried Pd (I.W.)/SSZ-13 (horizontal stripe fill) and (d) co-I.W. Pd and Mg on SSZ-13 (grid fill) catalysts which were then hydrothermally aged at 500 °C (HTA 500 C). Arrow indicates T_{90} was not reached by 600 °C. Feed Conditions: 9 % O_2, 6 % CO_2, 12 % H_2O, 2000 ppm CO, 500 ppm NO, 3000 ppm CH_4.

Table 4
CO-pulse chemisorption on selected Al_2O_3 supported methane oxidation catalysts.

Samples[a]	CO Consumed (μmol/g)	Dispersion (%)	Particle Size (nm)	Active metal surface area (m^2/g)	L_1/L_2[b] Ratio
Pd/Al_2O_3 Fresh	2.3	48	1.9	1.00	3.8
Pd/Al_2O_3 HTA 500 C	2.2	46	2.0	0.96	3.3
Pd+Mg/ Al_2O_3 HTA 500 C	1.9	40	2.3	0.82	2.3
Pd/Al_2O_3 HTA 700 C	1.7	36	2.5	0.74	1.9
Pd+Mg/ Al_2O_3 HTA 700 C	1.7	36	2.5	0.74	2.5

[a] Pd:Mg is 1:1 molar ratio for all bimetallic samples, Mg added sequentially via I.W.
[b] $L_1/L_2 \equiv$ Pd(1 0 0)/Pd(1 1 1) estimated from CO TPD.

using H_2 prior to exposure to CO pulses.

High dispersion of Pd was observed on fresh Pd/Al_2O_3 at 48 % and was used as a reference. Mild hydrothermal aging of Pd/Al_2O_3 at 500 °C did not significantly affect the Pd dispersion. However, incorporation of Mg into the mildly aged sample lowered the Pd dispersion from 46 % to 40 %, possibly due to an increase in particle size as a result of additional hydrothermal aging at 500 °C or a fraction of the Pd particles being covered by a MgO layer limiting access of CO to Pd sites.

Exposing Pd/Al_2O_3 to severe hydrothermal aging conditions at 700 °C for 15 h caused a decrease in Pd dispersion to 36 % accompanied by further increase in Pd particle size from 1.9 nm to 2.5 nm. It is noteworthy that the Mg incorporation in the severely aged Pd+Mg/ Al_2O_3 HTA 700 C sample did not lead to further deterioration in Pd dispersion or particle size even after being subjected to hydrothermal aging at 700 °C twice for a total of 30 h. Thus, Mg incorporation to severely aged Pd/Al_2O_3 prevented any further loss of accessible Pd/PdOx active sites, helping retain the size of Pd particles upon additional aging at 700 °C.

3.1.3.2. CO and CO_2 temperature-programmed desorption (TPD). Temperature programmed desorption after CO-pulse chemisorption can provide valuable insight into the type of Pd active sites based on their CO binding strength similar to those discussed for the SSZ-13 supported catalysts. For the samples supported on Al_2O_3, the low temperature CO desorption feature between 90 °C and 150 °C (L_1) and the high temperature CO desorption peak in the 300–350 °C range (L_2) in Fig. 7(a) indicate two distinct CO desorption sites which are attributed to CO linearly bound on Pd (1 0 0) and Pd (1 1 1), respectively [47,48]. Presence of Pd (1 0 0) is also suggested by the evolution of CO_2 during CO desorption in the temperature range shown in Fig. 7(b) which is typically due to disproportionation of CO on Pd (1 0 0) facets [48]. As discussed in the context of SSZ-13 supported catalysts, methane oxidation via Mars-van Krevelen mechanism is favored on Pd (1 0 0), the relative ratio of the CO desorption features (L_1/L_2) corresponding to Pd (1 0 0)/Pd (1 1 1) in Table 4 can provide useful insights into samples that are likely to have promising methane oxidation efficacy. In general, alumina supported catalysts demonstrated higher L_1/L_2 ratio than SSZ-13 supported catalysts with the proportion of Pd (1 0 0) being at least ~2 times higher than Pd (1 1 1) in the Al_2O_3 catalysts suggesting superior methane oxidation activity [49].

3.1.3.3. H_2 temperature programmed reduction (TPR). To investigate the reducibility of the Pd/PdOx active sites in the alumina supported methane oxidation catalysts, H_2-TPR was conducted on the samples (Fig. 7(c) and (d)). The alumina supported samples demonstrated H_2 consumption below 20 °C indicative of a sharp reduction of PdOx, while the presence of palladium hydride (PdH_x) was indicated by the negative peaks seen between 30 °C and 50 °C. A broad reduction feature at ~300 °C could be ascribed to reduction of Pd particles or two-dimensional surface PdOx complexes strongly interacting with the support [51,78–81].

While the H_2 consumption during TPR for the alumina supported samples have similar general features, there are subtle differences between the reducibility of the active sites based on the sample aging history and presence of Mg which are more apparent at an enlarged scale in the narrow temperature window shown in Fig. 7(d). A shift in the PdOx reduction peaks of the H_2- TPR profile correlate with an increase in interaction with the support. The sharp low-temperature feature (PdO-a) is attributed to larger, more reducible PdOx particles than those represented by the higher temperature shoulder (PdO-b) [20,79].

In the fresh Pd/Al_2O_3, larger PdOx particles are reduced at − 3 °C (PdO-a) and relatively smaller ones at 16 °C (PdO-b). A change in PdOx particle size distribution in Pd/Al_2O_3 HTA 500 C is suggested by the increased contribution to the shoulder PdO-b reduction feature after hydrothermal aging at 500 °C in the presence of excess oxygen. Chen and Ruckenstein proposed that on thermal treatment in oxygen at temperature above 350 °C, smaller PdOx crystallites start to spread which can lead to stronger interaction with the support [82]. Lieske and Volter also reported initiation of redistribution of Pd/PdOx particles under oxidative treatment at temperatures as low as 400 °C [78]. As the reduction temperatures of PdO-a and PdO-b remained unchanged after mild aging, the PdOx particle sizes are likely similar to that of fresh Pd/Al_2O_3 sample even though the size distribution of Pd/Al_2O_3 HTA 500 C may have altered on exposure to oxidizing environment at 500 °C. Mg incorporation into Pd/Al_2O_3 HTA 500 C, however, pushed the PdO-a and PdO-b peaks to somewhat higher temperatures of 2 °C and 18 °C, respectively, signifying a slight increase in stability of PdOx in the resulting sample. While additional aging at 500 °C could result in

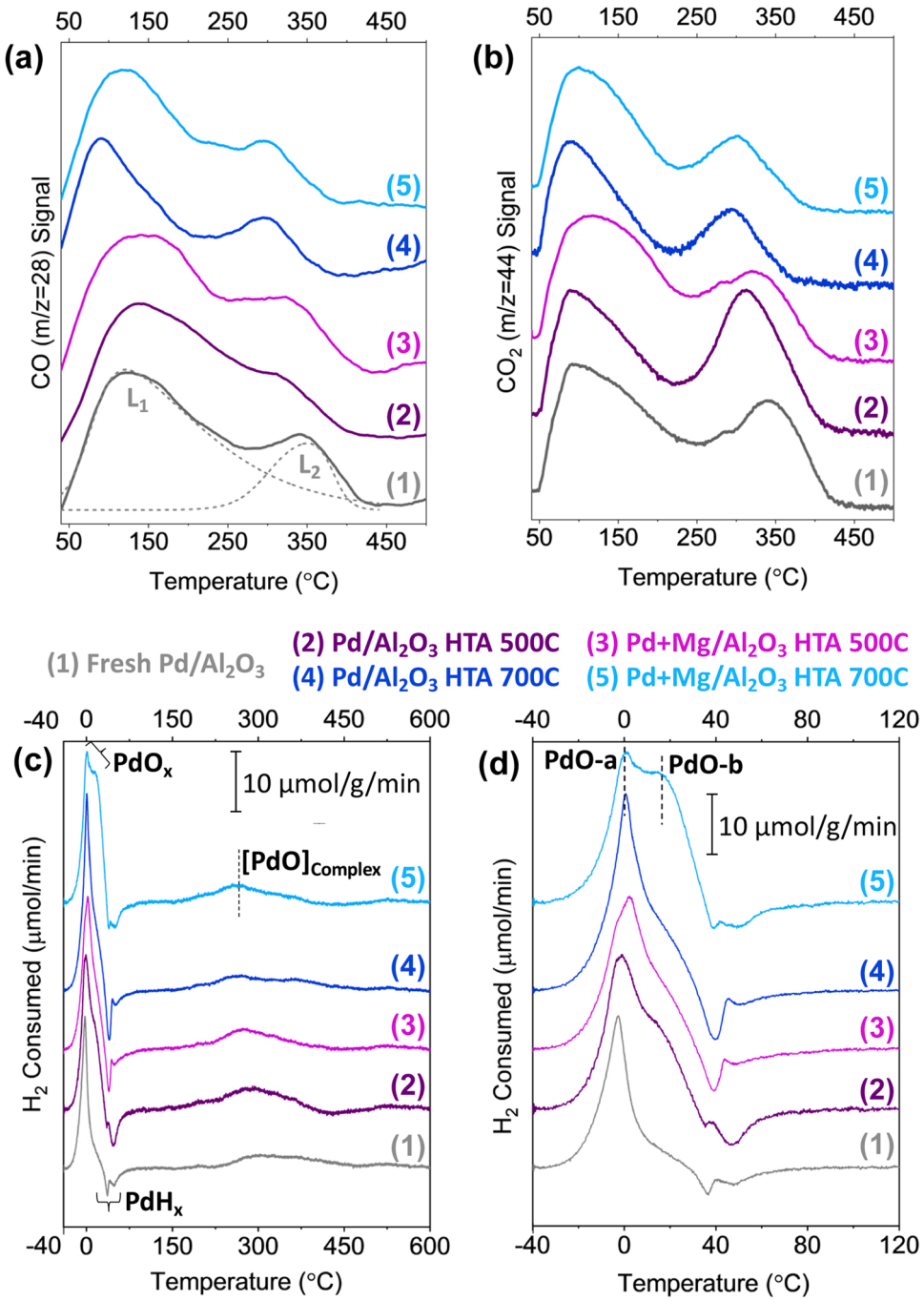

Fig. 7. (a) CO (*m/z* 28) and (b) CO_2 (*m/z* 44) during temperature-programmed desorption following CO-pulse chemisorption where dotted gray lines show peaks L_1 and L_2 obtained by deconvolution of the CO TPD profile for the catalyst; and (c) H_2-TPR profiles from − 40 °C to 600 °C with (d) Zoom in of low temperature TPR peaks between − 40 °C to 120 °C for the Al_2O_3 samples.

further fragmentation of PdOx crystallites, another factor that may play a role in the case of Pd+Mg/Al_2O_3 HTA 500 C catalyst is interaction with electropositive Mg, perhaps at the interfacial region, which can have a stabilizing effect on PdOx particles [40,82].

The comparative increase in PdOx reduction temperatures was observed for the Pd/Al_2O_3 HTA 700 C catalyst than the HTA 500 C catalysts, which suggests more cavity formation, rupturing and scattering of PdOx crystallites occurred on exposure to the severe hydrothermal aging conditions at 700 °C for 15 h [49,66]. The change in reduction temperature for Pd/Al_2O_3 HTA 700 C was also accompanied by a relative increase in intensity of the corresponding PdO-a feature indicating that some of the smaller PdOx particles formed due to fragmentation may have agglomerated upon severe aging. Interestingly, further shift in PdOx reduction peaks to higher temperatures was not detected on Mg addition to Pd/Al_2O_3 HTA 700 C, despite the catalyst being subjected to severe aging conditions at 700 °C for a total of 30 h, suggesting resistance to additional sintering of the comparatively smaller PdOx particles in the presence of Mg. Moreover, the substantial increase of the PdO-b reduction feature in Pd+Mg/Al_2O_3 HTA 700 C indicated a significant alteration of PdOx interaction with the support compared to the Mg-free Pd/Al_2O_3 HTA 700 C sample. This change in the support interaction may be associated with an improved interaction of PdOx with electropositive Mg during surface roughening and restructuring of PdOx crystallites on exposure to severe aging under

oxidizing conditions that could lead to redispersion of PdOx species [46,66,78].

Furthermore, two negative PdH_x peaks between 30 °C and 50 °C were observed for the alumina supported samples in Fig. 7(c) and (d). The temperature of PdH_x decomposition typically depends on the size of the Pd particle on which the hydride was formed [80]. Hydrides formed on smaller Pd particles decompose at lower temperatures than those formed on larger Pd particles. Redistribution of PdOx particles with aging conditions and Mg incorporation was further highlighted by the changing PdH_x features observed in the TPR profile for the alumina supported catalysts investigated.

3.1.4. Evaluation of CH_4 oxidation activity under simulated-engine exhaust conditions

In order to gain insights into how traditional oxidation catalysts such as Pd/Al_2O_3 compare with Pd (I.W.)/SSZ-13 catalysts in terms of methane conversion efficiency under lean conditions, Pd/Al_2O_3 was hydrothermally aged at 500 °C and its methane light-off behavior was investigated. After aging, Pd/Al_2O_3 demonstrated promising lean methane oxidation activity under synthetic exhaust conditions with both T_{50} and T_{90} for methane conversion being lower than Pd (I.W.)/SSZ-13 HTA 500 C (ΔT_{50} ~111 °C and ΔT_{90} ~167 °C) as observed in Fig. 8. For the same Pd loading (1 wt%), Pd/PdOx particles on Al_2O_3 were likely more accessible than those on SSZ-13 supported catalysts as evidenced by H_2 TPR. High temperature hydrothermal aging of Pd based zeolites can potentially lead to migration of a fraction of the Pd particles into the zeolite cage and result in partial loss of PdOx particles due to transformation to cationic Pd at the ion-exchange sites within the zeolite [60,61]. The higher methane conversion efficiency of Pd/Al_2O_3 compared to Pd (I.W.)/SSZ-13 provides further indication of Pd/PdOx particles being more effective at methane oxidation compared to Pd cations considering that the CO TPD and H_2 TPR experiments suggest that the Pd/Al_2O_3 catalyst would only have Pd/PdOx particles on the surface.

3.1.4.1. Effect of Mg addition on hydrothermal stability of Pd/Al_2O_3.

While the alumina catalyst demonstrated promising activity after mild hydrothermal exposure, longer term aging may provide a more definitive understanding of its durability. Pd/Al_2O_3 was thus exposed to 10 % water vapor at 700 °C for 15 h (HTA 700 C) under lean conditions prior to performance evaluation under synthetic exhaust conditions. Comparison of methane oxidation activity between Pd/Al_2O_3 HTA 500 C and Pd/Al_2O_3 HTA 700 C in Fig. 9(i)(b) and (i)(c) shows an increase in both T_{50} (ΔT_{50} ~8 °C) and T_{90} (ΔT_{90} ~25 °C) when the catalyst was subjected to the more severe HTA 700 C. The light-off curve for fresh Pd/Al_2O_3 included in Fig. 9(i) for reference shows an onset of methane oxidation at lower temperatures but a deterioration in catalyst activity on prolonged exposure to reaction conditions, leading to high T_{90} comparable to the severely aged sample suggesting an improvement in the catalyst active sites occurred after mild HTA exposure.

The CO desorption experiments showed that the Pd (1 0 0)/ Pd (1 1 1) ratio (L_1/L_2 in Table 4) in the Pd/Al_2O_3 HTA 500 C sample was lower compared to the fresh Pd/Al_2O_3 with little change to particle size and dispersion suggesting that a combination of these factors likely impact the lean light-off behavior of methane on a catalyst. The severe HTA exposure that Pd/Al_2O_3 HTA 700 C experienced, resulted in a more significant drop in the L_1/L_2 ratio and dispersion of the Pd/PdOx particles likely resulting in fewer available active sites leading to lesser low temperature methane conversion.

Mg was incorporated sequentially by I.W. into both the mild and severe hydrothermally aged Pd/Al_2O_3 samples, and the resulting catalysts were subjected to further hydrothermal aging at 500 °C and 700 °C, respectively, before methane conversion testing. It is important to note that the differences in the mild and severe HTA exposures was not only temperature but also in the exposure time at the elevated temperatures such that $Pd+Mg/Al_2O_3$ HTA 500 C was exposed to aging conditions for a total of 8 h while the $Pd+Mg/Al_2O_3$ HTA 700 C sample was subjected to aging conditions for a total of 30 h. For the HTA 500 C catalyst, the addition of Mg resulted in small increases in the T_{50} and T_{90}, respectively (Fig. 9(i)(b) and (i)(d)). However, the Mg addition step was found to improve the hydrothermal stability and methane oxidation activity for the HTA 700 C catalyst lowering the T_{50} and T_{90}. The nearly identical activity measured for $Pd+Mg/Al_2O_3$ HTA 500 C and $Pd+Mg/Al_2O_3$ HTA 700 C (Fig. 9(i)(d) and (i)(e)) suggests a stabilizing improvement to the Pd/Al_2O_3 occurs when Mg is added followed by a HTA exposure [83].

High temperature exposure of Al_2O_3 supported catalysts could result in loss of methane oxidation activity due to drop in dispersion of the Pd/PdOx particles on the catalyst surface as suggested by CO chemisorption experiments. Mg incorporation to Pd/Al_2O_3 was found to inhibit further loss in dispersion of the Pd/PdOx species on Al_2O_3 on additional aging at 700 ºC (Table 4). Further aging, as in the case of Mg-containing catalyst (HTA 700 C), can lead to restructuring of PdOx particles due to surface roughening indicated by H_2 TPR which can, in turn, impact the binding strength of the reactants and activity of surface oxygen [45,66]. CO and CO_2 TPD experiments show that during restructuring of the PdOx

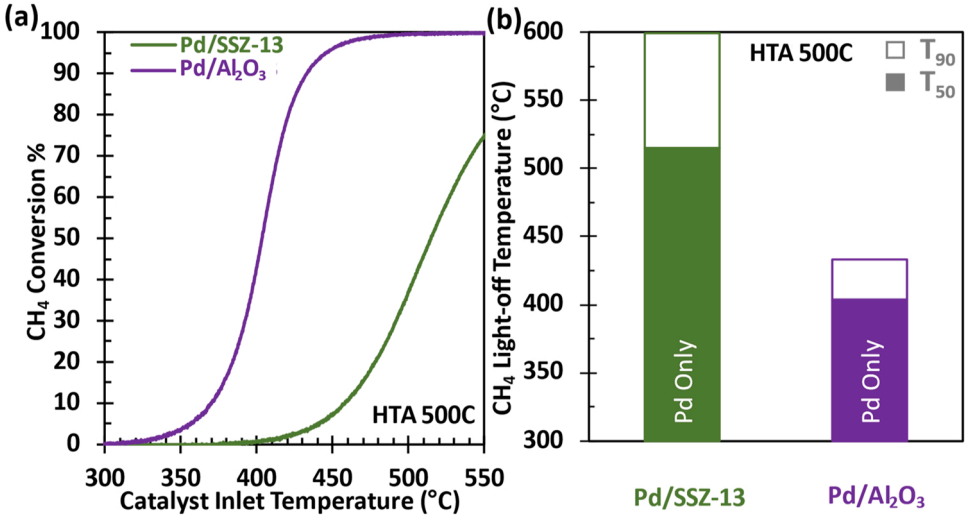

Fig. 8. Comparison of CH_4 (a) light-off curves and (b) T_{50} and T_{90} light-off temperatures on Pd (I.W.)/SSZ-13 and Pd/Al_2O_3 after hydrothermal treatment at 500 °C (HTA 500 C). Feed Conditions: 9 % O_2, 6 % CO_2, 12 % H_2O, 2000 ppm CO, 500 ppm NO, 3000 ppm CH_4.

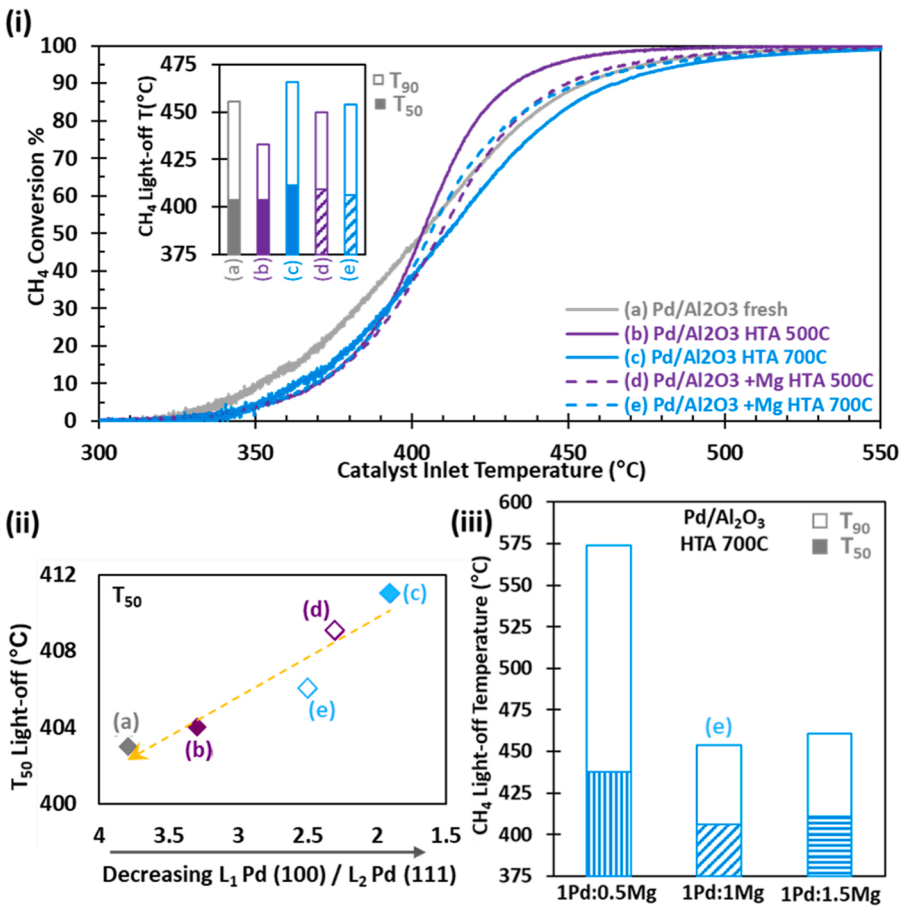

Fig. 9. (i) CH_4 light-off curves with T_{50} and T_{90} temperatures in inset, and (ii) CH_4 oxidation T_{50} correlated with Pd (1 0 0)/Pd (1 1 1) ratio (L_1/L_2) obtained from the CO-TPD profiles for (a) Pd/Al_2O_3 Fresh, (b) Pd/Al_2O_3 HTA 500 C, (c) Pd/Al_2O_3 HTA 700 C, (d) $Pd+Mg/Al_2O_3$ HTA 500 C, and (e) $Pd+Mg/Al_2O_3$ HTA 700 C. (iii) CH_4 oxidation T_{50} and T_{90} for $Pd+Mg/Al_2O_3$ HTA 700 C catalysts with 0.5 Pd:1Mg (vertical stripes fill), 1 Pd:1Mg (diagonal stripes fill) and 1 Pd:1.5Mg (horizontal stripes fill) ratios. Feed Conditions: 9 % O_2, 6 % CO_2, 12 % H_2O, 2000 ppm CO, 500 ppm NO, 3000 ppm CH_4.

particles, preferential Pd facets active for methane oxidation can be exposed [45,46,49,66].

As methane oxidation has been reported to occur via the Mars-van Krevelen mechanism on Pd-based catalysts, the reactivity of surface oxygen also plays an important role in the activity of the catalyst for methane oxidation ([32,46] and references therein). Electropositive Mg incorporation into Pd/Al_2O_3 could potentially aid the formation of active Pd/PdOx facets with enhanced oxygen-exchange capability during restructuring under severe hydrothermal conditions leading to superior thermal stability while maintaining the methane oxidation activity of the resulting catalyst [49,84]. Fig. 9 (ii) highlights the increase in T_{50} for methane oxidation for the alumina supported samples as the Pd (1 0 0) to Pd (1 1 1) ratio (L_1/L_2 in Table 4) within a specific sample decrease. With increase in severity of hydrothermal aging from 500 °C for 4 h to 700 °C for 15 h, the L_1/L_2 ratio of Pd/Al_2O_3 significantly reduced likely due to sintering of Pd/PdOx particles possibly increasing the proportion of highly coordinated Pd (1 1 1) in the Pd/Al_2O_3 HTA 700 C sample. While incorporation of Mg to Pd/Al_2O_3 HTA 500 C decreased the L_1/L_2 ratio, addition of Mg to the severely aged Pd/Al_2O_3 HTA 700 C increased the L_1/L_2 ratio. These observations suggest that the presence of Mg during surface roughening and restructuring of Pd/PdOx on exposure to high temperature hydrothermal conditions (700 °C, 30 h) leads to preferential formation methane oxidation active Pd (1 0 0), resulting in catalysts with improved hydrothermal stability.

In general, alumina supported catalysts demonstrated higher L_1/L_2 ratio than SSZ-13 supported catalysts with the proportion of Pd (1 0 0) being at least ~2 times higher than Pd (1 1 1) in the former samples correlating well with the lower T_{50} for methane oxidation observed in the alumina supported catalysts irrespective of their aging history.

3.1.4.2. Impact of Mg to Pd ratio on CH_4 oxidation activity. The molar ratio of Pd to Mg in all of the $Pd+Mg/Al_2O_3$ catalysts discussed in the previous sections was 1:1. To understand the influence of Pd to Mg ratio on methane conversion, the ratio of Pd:Mg added to Pd/Al_2O_3 HTA 700 C was varied to include ratios of 1:0.5, 1:1 and 1:1.5. After addition of Mg the catalysts were subjected to a second HTA 700 C (total 30 h HTA exposure) and were then evaluated for methane oxidation efficacy under the same synthetic exhaust conditions.

Fig. 9 (iii) showed that increasing the level of Mg in the Pd/Al_2O_3 resulted in lowering the T_{50} for methane oxidation up to 1 Pd:1Mg ratio. Additional benefits in lowering the T_{50} or T_{90} for methane conversion were not observed when the Mg level was increased further to obtain 1 Pd:1.5Mg in the $Pd+Mg/Al_2O_3$ HTA 700 C catalyst. Thus, the 1 Pd:1Mg ratio in the $Pd+Mg/Al_2O_3$ catalyst demonstrated superior hydrothermal stability as well as promising activity for methane oxidation under lean synthetic exhaust conditions.

3.2. Catalyst kinetics

For selected methane oxidation catalyst samples probed using CO-pulses in this study, turnover frequencies (TOF) at 20 % conversion of methane were also calculated. Fig. 10 shows higher TOF correlation with increasing Pd/PdOx particle size. This correlation is consistent with the Mars-van Krevelen mechanism for methane oxidation which illustrates how smaller PdOx particles have stronger Pd-O bonds which in turn cause a reduction in the density of the oxygen vacancies available to achieve higher methane TOF via catalytic redox cycles [20]. Briot and Primet have also reported increases in TOF with particle size for aged Pd/Al_2O_3 samples, albeit in the absence of excess water in the reaction feed and at lower methane conversion [85]. Investigations by Murata et al. showed similar monotonic increase in TOF in the presence of 12 %

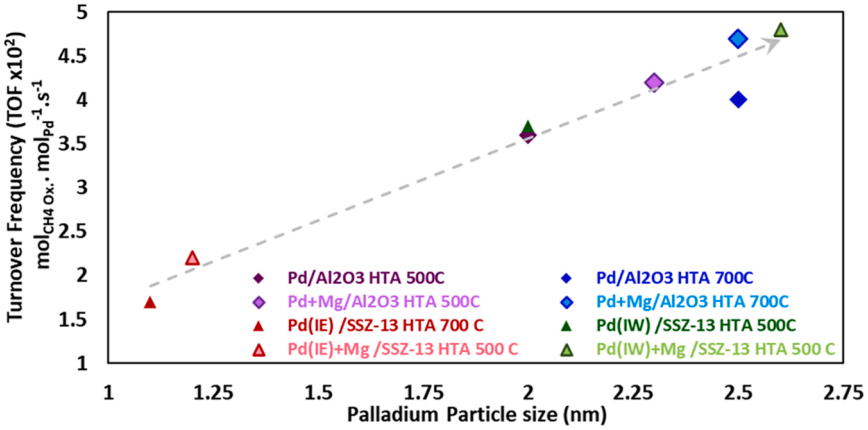

Fig. 10. Turnover frequency (TOF) at 20 % methane oxidation of alumina supported (diamond markers) and SSZ-13 -supported (triangle markers) catalysts vs. particle size of palladium obtained from CO chemisorption. Mg-incorporated samples indicated with corresponding bordered markers.

water under lean conditions until Pd particle size ~7 nm [27]. Additional kinetic parameters from the Arrhenius equation were estimated from methane oxidation light-off curves of the selected catalysts below 20 % conversion of methane assuming first order reaction and are presented in Table 5.

Apparent activation energies for methane conversion below 20 % for the hydrothermally aged methane oxidation catalysts presented herein are within the range of 139–182 kJ/mol under full synthetic engine-exhaust conditions. At less than 3–5 % methane conversions, typically in the absence of excess water or other inhibiting constituent of the feed, apparent activation energies in the range of 75–180 kJ/mol have been reported for other Pd supported catalytic systems [33,34,65].

It is well established that methane oxidation is strongly inhibited in the presence of excess water typical of lean-burn, natural gas engine exhaust, and that water desorption from the active sites of the catalyst is the rate determining step for methane activation under wet conditions [19,26,86]. In addition to water, other constituents of engine-exhaust as well as products of oxidation, such as CO_2, CO and NO, have also been shown to hinder methane oxidation due to competitive adsorption of species on catalyst active sites [20,33,34]. It is therefore not surprising that these new catalysts tested under the full exhaust condition indicated apparent activation energies on the higher end of the range.

Table 5
Methane oxidation kinetics parameters and turn-over frequencies.

Samples (Pd: Mg molar ratio 1:1)	Arrhenius Equation Parameters[a]		At 20 % CH_4 Oxidation	
	$E_{A_{apparent}}$ (kJ/mol)	A x10^{10} $\left(\frac{mol_{CH_4Ox.}}{g_{cat}.s}\right)$	Catalyst Bed (°C)	TOF x10^2 $\left(\frac{mol_{CH_4Ox.}}{mol_{Pd}.s}\right)$
Alumina Supported Catalysts				
Pd/Al_2O_3 HTA 500 C	159	5.1	392	3.6
$Pd+Mg/Al_2O_3$ HTA 500 C	172	45	395	4.2
Pd/Al_2O_3 HTA 700 C[b]	163	20	385	4.0
$Pd+Mg/Al_2O_3$ HTA 700 C	167	9	410	4.7
SSZ-13 Supported Catalysts				
Pd(I.W.)/SSZ-13 HTA 500 C	182	5.8	484	3.7
Pd(I.W.)+Mg/SSZ-13 HTA 500 C	150	0.05	473	4.8
Pd(I.E.)/SSZ-13 HTA 700 C[b]	153	0.4	429	1.7
Pd(I.E.)+Mg/SSZ-13 HTA 700 C	139	0.0006	568	2.2

[a] Calculated from 1 % to 20 % CH_4 conversion.
[b] Calculated from 3 % to 20 % CH_4 conversion.

4. Conclusions

Mg was incorporated followed by a hydrothermal treatment (i.e. Mg addition step) into either SSZ-13 or alumina supported Pd catalysts and its effect on methane oxidation activity under synthetic exhaust conditions relevant to lean-burn natural gas engines were investigated. The major conclusion of this study was that the Mg addition step improved the hydrothermal durability of the Pd/PdOx containing catalysts used in this study. Additional valuable information was also gained about the impact of the catalyst support, aging conditions, and Mg addition steps on the state of active Pd/PdOx sites for methane oxidation from catalyst characterization with H_2 TPR, CO-pulse chemisorption and CO/CO_2 TPD.

For SSZ-13 supported catalysts:

- Higher Pd/PdOx particle formation and lower T_{90} in Pd/SSZ-13 synthesized by I.W. compared to I.E. indicated that Pd/PdOx particles were better than cationic Pd^{2+} for methane oxidation under lean exhaust-relevant conditions.
- The Mg addition step to Pd (I.W.)/SSZ-13 was beneficial in lowering both T_{50} and T_{90} for lean methane oxidation and was correlated with the formation of highly reducible, active Pd/PdOx sites outside the zeolite cage suggesting that Mg may prevent excessive agglomeration of the particles.

For alumina supported catalysts:

- Hydrothermally aged Pd/Al_2O_3 catalysts demonstrated significantly higher activity for methane oxidation compared to both I.E. and I.W. Pd/SSZ-13 catalysts in this study further supporting the importance of high dispersion of Pd/PdOx particles
- Mg addition step improved MOC activity for the severely aged Pd/Al_2O_3 (HTA700C) sample further supporting its stabilizing impact to the Pd/PdOx particles.
- Catalyst characterization suggested that the improved lean CH_4 oxidation activity and hydrothermal stability of $Pd+Mg/Al_2O_3$ HTA 700 C was due to the influence of Mg during surface roughening and restructuring of Pd/PdOx on severe hydrothermal aging which can lead to active Pd (1 0 0) facets being preferentially exposed in addition to hindering excessive sintering.
- The benefit of Mg addition was not found to exist until it reached a 1:1 Mg:Pd molar ratio with no further improvement observed with further Mg addition.

CRediT authorship contribution statement

Sreshtha Sinha Majumdar conducted the activity experiments, planned characterization experiments, analyzed the data and wrote the manuscript. **Melanie Moses-DeBusk** contributed ideas to the concept, lead the project, synthesized the catalysts, reviewed the manuscript. **Dhruba Jyoti Deka** conducted and analyzed the characterization experiments and contributed to writing corresponding sections of the manuscript. **Michelle Kidder** performed physisorption analysis for surface area and pore size for selected samples. **Calvin R. Thomas** conducted activity experiments on SSZ-13 samples. **Josh Pihl** contributed ideas to the concept and reviewed the manuscript.

Declaration of Competing Interest

The authors declare the following financial interests/personal relationships which may be considered as potential competing interests: Melanie Moses-DeBusk, Sreshtha Sinha Majumdar, Josh A. Pihl have a pending patent application titled Hydrothermally Stable Methane Oxidation Catalyst assigned to UT-Battelle, LLC.

Data availability

Data will be made available on request.

Acknowledgements

This research was supported by the Department of Energy (DOE), Office of Energy Efficiency and Renewable Energy (EERE) and Vehicle Technologies Office (VTO) and used resources at the National Transportation Research Center, a DOE-EERE User Facility at Oak Ridge National Laboratory. The authors gratefully acknowledge guidance and support from Kevin Stork and Gurpreet Singh at DOE VTO.

Appendix A. Supporting information

Supplementary data associated with this article can be found in the online version at doi:10.1016/j.apcatb.2023.123253.

References

[1] H.T. Adam Barth, Jamie Brick, Dumitru Dediu, The Future of Natural Gas in North America, McKinsey & Company. (2020).
[2] E.J. Moniz, H.D. Jacoby, A.J.M. Meggs, The Future of Natural Gas - MIT Study, 2011.
[3] G. Caravaggio, L. Nossova, M.J. Turnbull, Nickel-magnesium mixed oxide catalyst for low temperature methane oxidation, Chem. Eng. J. 405 (2021), 126862.
[4] M.A. Mac Kinnon, J. Brouwer, S. Samuelsen, The role of natural gas and its infrastructure in mitigating greenhouse gas emissions, improving regional air quality, and renewable resource integration, Prog. Energy Combust. Sci. 64 (2018) 62–92.
[5] F.-Y. Liang, M. Ryvak, S. Sayeed, N. Zhao, The role of natural gas as a primary fuel in the near future, including comparisons of acquisition, transmission and waste handling costs of as with competitive alternatives, Chem. Cent. J. 6 (2012) 1–24.
[6] K. Kohse-Höinghaus, Clean combustion: chemistry and diagnostics for a systems approach in transportation and energy conversion, Prog. Energy Combust. Sci. 65 (2018) 1–5.
[7] A. Safari, N. Das, O. Langhelle, J. Roy, M. Assadi, Natural gas: a transition fuel for sustainable energy system transformation? Energy Sci. Eng. 7 (2019) 1075–1094.
[8] J.J. López, R. Novella, J. Gomez-Soriano, P.J. Martinez-Hernandiz, F. Rampanarivo, C. Libert, M. Dabiri, Advantages of the unscavenged pre-chamber ignition system in turbocharged natural gas engines for automotive applications, Energy 218 (2021).
[9] J. Kheyrollahi, S. Jafarmadar, S. Khalilarya, S.R. Amini, Niaki, Improvement of performance and emission in a lean-burn gas fueled spark ignition engine by using a new pre-chamber, Environ. Prog. Sustain Energy (2021).
[10] D. Jiang, K. Khivantsev, Y. Wang, Low-temperature methane oxidation for efficient emission control in natural gas vehicles: Pd and beyond, ACS Catal. 10 (2020) 14304–14314.
[11] X. Duan, B. Deng, Y. Liu, S. Zou, J. Liu, R. Feng, An experimental study the impact of the hydrogen enrichment on cycle-to-cycle variations of the large bore and lean burn natural gas spark-ignition engine, Fuel 282 (2020), 118868.
[12] X. Duan, B. Deng, Y. Liu, Y. Li, J. Liu, Experimental study the impacts of the key operating and design parameters on the cycle-to-cycle variations of the natural gas SI engine, Fuel 290 (2021), 119976.
[13] S. Sinha Majumdar, A.-M. Alexander, P. Gawade, G. Celik, U.S. Ozkan, Effect of alumina incorporation on the sulfur tolerance of the dual-catalyst aftertreatment system for reduction of nitrogen oxides under lean conditions, Catal. Today 320 (2019).
[14] N. Peters, S.K.P. Subramanyam, M. Bunce, H. Blaxill, J. Pihl, M. Moses-Debusk, G. Vishwanathan, D. Tew, Design and development of a high-efficiency single cylinder natural gas-fueled jet ignition engine, SAE Technical Papers, Part F1637 (2020).
[15] M. Cargnello, J.J. Delgado Jaén, J.C. Hernández Garrido, K. Bakhmutsky, T. Montini, J.J. Calvino Gámez, R.J. Gorte, P. Fornasiero, Exceptional activity for methane combustion over modular Pd@CeO2 subunits on functionalized Al2O3, Science 337 (2012) (1979) 713–717.
[16] R.J. Farrauto, Low-temperature oxidation of methane, Science 337 (2012) (1979) 659–660.
[17] A.E. Shilov, G.B. Shul'pin, Activation of C-H bonds by metal complexes, Chem. Rev. 97 (1997) 2879–2932.
[18] D. Roth, P. Gélin, M. Primet, E. Tena, Catalytic behaviour of Cl-free and Cl-containing Pd/Al2O3 catalysts in the total oxidation of methane at low temperature, Appl. Catal. A Gen. 203 (2000) 37–45.
[19] R. Burch, M.J. Hayes, C-H bond activation in hydrocarbon oxidation on solid catalysts, J. Mol. Catal. A Chem. 100 (1995) 13–33.
[20] K.I. Fujimoto, F.H. Ribeiro, M. Avalos-Borja, E. Iglesia, Structure and reactivity of PdOx/ZrO2 catalysts for methane oxidation at low temperatures, J. Catal. 179 (1998) 431–442.
[21] A.P. Ladshaw, S. Sinha Majumdar, J.A. Pihl, Experiments and modeling to evaluate global reaction kinetics of three-way catalyst light off for net-zero carbon fuels and selected fuel blends, Appl. Catal. B 324 (2023), 122281.
[22] D. Dissanayake, J.H. Lunsford, M.P. Rosynek, Site differentiation in homolytic vs. Heterolytic activation of methane over Ba/MgO catalysts, J. Catal. 146 (1994) 613–615.
[23] P. Gélin, M. Primet, Complete oxidation of methane at low temperature over noble metal based catalysts: a review, Appl. Catal. B 39 (2002) 1–37.
[24] S. Sinha Majumdar, J.A. Pihl, Impact of selected high-performance fuel blends on three-way catalyst light off under synthetic spark-ignition engine-exhaust conditions, Energy Fuels (2020).
[25] G. Lapisardi, L. Urfels, P. Gélin, M. Primet, A. Kaddouri, E. Garbowski, S. Toppi, E. Tena, Superior catalytic behaviour of Pt-doped Pd catalysts in the complete oxidation of methane at low temperature, Catal. Today 117 (2006) 564–568.
[26] D. Ciuparu, M.R. Lyubovsky, E. Altman, L.D. Pfefferle, A. Datye, Catalytic combustion of methane over palladium-based catalysts, Catal. Rev. Sci. Eng. 44 (2002) 593–649.
[27] K. Murata, J. Ohyama, Y. Yamamoto, S. Arai, A. Satsuma, Methane combustion over Pd/Al2O3Catalysts in the presence of water: effects of Pd particle size and alumina crystalline phase, ACS Catal. 10 (2020) 8149–8156.
[28] S. Sinha Majumdar, G. Celik, U.S. Ozkan, Investigation of the effect of alumina binder addition to Pd/SO42–ZrO2 catalysts during sol-gel synthesis, Ind. Eng. Chem. Res. 55 (2016) 11445–11457.
[29] S. Sinha Majumdar, G. Celik, A.-M. Alexander, P. Gawade, U.S. Ozkan, In-situ incorporation of binder during sol-gel preparation of Pd-based sulfated zirconia for reduction of nitrogen oxides under lean-burn conditions: effect on activity and wash-coating characteristics, Appl. Catal. B 202 (2017).
[30] J. Bin Lim, D. Jo, S.B. Hong, Palladium-exchanged small-pore zeolites with different cage systems as methane combustion catalysts, Appl. Catal. B 219 (2017) 155–162.
[31] K. Murata, Y. Mahara, J. Ohyama, Y. Yamamoto, S. Arai, A. Satsuma, The metal–support interaction concerning the particle size effect of Pd/Al2O3 on methane combustion, Angew. Chem. Int. Ed. 56 (2017) 15993–15997.
[32] W.R. Schwartz, L.D. Pfefferle, Combustion of methane over palladium-based catalysts: support interactions, J. Phys. Chem. C 116 (2012) 8571–8578.
[33] F.H. Ribeiro, M. Chow, R.A.D. Betta, Kinetics of the complete oxidation of methane over supported palladium catalysts.pdf, J. Catal. 146 (1994) 537–544.
[34] R.E. Hayes, S.T. Kolaczkowski, P.K.C. Li, S. Awdry, The palladium catalysed oxidation of methane: reaction kinetics and the effect of diffusion barriers, Chem. Eng. Sci. 56 (2001) 4815–4835.
[35] A.W. Petrov, D. Ferri, O. Kröcher, J.A. Van Bokhoven, Design of stable palladium-based zeolite catalysts for complete methane oxidation by postsynthesis zeolite modification, ACS Catal. 9 (2019) 2303–2312.
[36] I. Friberg, N. Sadokhina, L. Olsson, The effect of Si/Al ratio of zeolite supported Pd for complete CH4 oxidation in the presence of water vapor and SO2, Appl. Catal. B 250 (2019) 117–131.
[37] I. Friberg, A. Wang, L. Olsson, Hydrothermal aging of pd/LTA monolithic catalyst for complete CH4 oxidation, Catalysts 10 (2020).
[38] L.F. Yang, C.K. Shi, X.E. He, J.X. Cai, Catalytic combustion of methane over PdO supported on Mg-modified alumina, Appl. Catal. B 38 (2002) 117–125.
[39] W. Hu, G. Li, J. Chen, F. Huang, M. Gong, L. Zhong, Y. Chen, Enhancement of activity and hydrothermal stability of Pd/ZrO2-Al2O3 doped by Mg for methane combustion under lean conditions, Fuel 194 (2017) 368–374.
[40] H. Yoshida, T. Nakajima, Y. Yazawa, T. Hattori, Support effect on methane combustion over palladium catalysts, Appl. Catal. B 71 (2007) 70–79.
[41] S. Sinha Majumdar, J.A. Pihl, T.J. Toops, Reactivity of novel high-performance fuels on commercial three-way catalysts for control of emissions from spark-ignition engines, Appl. Energy 255 (2019), 113640.

[42] K.G. Rappé, C. DiMaggio, J.A. Pihl, J.R. Theis, S.H. Oh, G.B. Fisher, J. Parks, V. G. Easterling, M. Yang, M.L. Stewart, K.C. Howden, Aftertreatment protocols for catalyst characterization and performance evaluation: low-temperature oxidation, storage, three-way, and NH 3 -SCR catalyst test protocols, Emiss. Control Sci. Technol. 5 (2019) 183–214.
[43] M. Thommes, K. Kaneko, A.V. Neimark, J.P. Olivier, F. Rodriguez-Reinoso, J. Rouquerol, K.S.W. Sing, Physisorption of gases, with special reference to the evaluation of surface area and pore size distribution (IUPAC Technical Report), Pure Appl. Chem. 87 (2015) 1051–1069.
[44] Y. Gu, R.P. Zelinsky, Y.-R. Chen, W.S. Epling, Investigation of an irreversible NOx storage degradation Mode on a Pd/BEA passive NOx adsorber, Appl. Catal. B 258 (2019), 118032.
[45] O. Demoulin, G. Rupprechter, I. Seunier, B. Le Clef, M. Navez, P. Ruiz, Investigation of parameters influencing the activation of a Pd/γ-alumina catalyst during mèthane combustion, J. Phys. Chem. B 109 (2005) 20454–20462.
[46] S.K. Matam, M.H. Aguirre, A. Weidenkaff, D. Ferri, Revisiting the problem of active sites for methane combustion on Pd/Al 2O3 by operando XANES in a lab-scale fixed-bed reactor, J. Phys. Chem. C 114 (2010) 9439–9443.
[47] I. Stará, V. Matolín, The influence of particle size on CO adsorption on Pd/alumina model catalysts, Surf. Sci. 313 (1994) 99–106.
[48] R.S. Monteiro, L.C. Dieguez, M. Schmal, The role of Pd precursors in the oxidation of carbon monoxide over Pd/Al2O3 and Pd/CeO2/Al2O3 catalysts, Catal. Today 65 (2001) 77–89.
[49] E. Garbowski, C. Feumi-Jantou, N. Mouaddib, M. Primet, Catalytic combustion of methane over palladium supported on alumina catalysts: evidence for reconstruction of particles, Appl. Catal. A Gen. 109 (1994) 277–291.
[50] H.A. Doan, M.K. Sharma, W.S. Epling, L.C. Grabow, From active-site models to real catalysts: importance of the material gap in the design of Pd catalysts for methane oxidation, ChemCatChem 9 (2017) 1594–1600.
[51] S.K. Matam, E.H. Otal, M.H. Aguirre, A. Winkler, A. Ulrich, D. Rentsch, A. Weidenkaff, D. Ferri, Thermal and chemical aging of model three-way catalyst Pd/Al 2O 3 and its impact on the conversion of CNG vehicle exhaust, Catal. Today 184 (2012) 237–244.
[52] C. Dai, Y. Li, C. Ning, W. Zhang, X. Wang, C. Zhang, The influence of alumina phases on the performance of Pd/Al2O3 catalyst in selective hydrogenation of benzonitrile to benzylamine, Appl. Catal. A Gen. 545 (2017) 97–103.
[53] B.J. Adelman, W.M.H. Sachtler, The effect of zeolitic protons on NO(x) reduction over Pd/ZSM-5 catalysts, Appl. Catal. B 14 (1997) 1–11.
[54] W. Zhang, Y. Zhu, S. Niu, Y. Li, A study of furfural decarbonylation on K-doped Pd/Al2O 3 catalysts, J. Mol. Catal. A Chem. 335 (2011) 71–81.
[55] C. Fan, L. Yang, L. Luo, Z. Wu, Z. Qin, H. Zhu, W. Fan, J. Wang, A highly active Pd/H-ZSM-5 catalyst in lean methane combustion prepared: via a sol-gel method and treated by reduction-oxidation, New J. Chem. 44 (2020) 3940–3949.
[56] D. Ciuparu, M.R. Lyubovsky, E. Altman, L.D. Pfefferle, A. Datye, Catalytic combustion of methane over palladium-based catalysts, Catal. Rev. Sci. Eng. 44 (2002) 593–649.
[57] Y. Li, J.N. Armor, Catalytic combustion of methane over palladium exchanged zeolites, Appl. Catal. B 3 (1994) 275–282.
[58] R. Gholami, K.J. Smith, Activity of PdO/SiO2 catalysts for CH4 oxidation following thermal treatments, Appl. Catal. B 168-169 (2015) 156–163.
[59] X. Chen, Y. Cheng, C.Y. Seo, J.W. Schwank, R.W. McCabe, Aging, re-dispersion, and catalytic oxidation characteristics of model Pd/Al2O3 automotive three-way catalysts, Appl. Catal. B 163 (2015) 499–509.
[60] Y.S. Ryou, J. Lee, S.J. Cho, H. Lee, C.H. Kim, D.H. Kim, Activation of Pd/SSZ-13 catalyst by hydrothermal aging treatment in passive NO adsorption performance at low temperature for cold start application, Appl. Catal. B 212 (2017) 140–149.
[61] J. Lee, J. Kim, Y. Kim, S. Hwang, H. Lee, C.H. Kim, D.H. Kim, Improving NOx storage and CO oxidation abilities of Pd/SSZ-13 by increasing its hydrophobicity, Appl. Catal. B 277 (2020), 119190.
[62] H. Maeda, Y. Kinoshita, K.R. Reddy, K. Muto, S. Komai, N. Katada, M. Niwa, Activity of palladium loaded on zeolites in the combustion of methane, Appl. Catal. A Gen. 163 (1997) 59–69.
[63] Y.S. Ryou, J. Lee, H. Lee, C.H. Kim, D.H. Kim, Effect of various activation conditions on the low temperature NO adsorption performance of Pd/SSZ-13 passive NOx adsorber, Catal. Today 320 (2019) 175–180.
[64] H.Y. Chen, J. Lu, J.M. Fedeyko, A. Raj, Zeolite supported Pd catalysts for the complete oxidation of methane: a critical review, Appl. Catal. A Gen. 633 (2022).
[65] Y. Cui, J. Zhu Chen, B. Peng, L. Kovarik, A. Devaraj, Z. Li, T. Ma, Y. Wang, J. Szanyi, J.T. Miller, Y. Wang, F. Gao, Onset of high methane combustion rates over supported palladium catalysts: from isolated Pd cations to PdO nanoparticles, JACS Au 1 (2021) 396–408.
[66] A.K. Datye, J. Bravo, T.R. Nelson, P. Atanasova, M. Lyubovsky, L. Pfefferle, Catalyst microstructure and methane oxidation reactivity during the Pd↔PdO transformation on alumina supports, Appl. Catal. A Gen. 198 (2000) 179–196.
[67] R.J. Farrauto, M.C. Hobson, T. Kennelly, E.M. Waterman, Catalytic chemistry of supported palladium for combustion of methane, Appl. Catal. A Gen. 81 (1992) 227–237.
[68] R. Burch, M.J. Hayes, CH bond activation in hydrocarbon oxidation on solid catalysts, J. Mol. Catal. A Chem. 100 (1995) 13–33.
[69] C. Li, G. Li, Q. Xin, FT-IR spectroscopic studies of methane adsorption on magnesium oxide, J. Phys. Chem. 98 (1994) 1933–1938.
[70] A. Moral, I. Reyero, J. Llorca, F. Bimbela, L.M. Gandía, Partial oxidation of methane to syngas using Co/Mg and Co/Mg-Al oxide supported catalysts, Catal. Today 333 (2019) 259–267.
[71] M. Chen, H. Zheng, C. Shi, R. Zhou, X. Zheng, Synthesis of nanoparticle Ce-Mg-O mixed oxide as efficient support for methane oxidation, J. Mol. Catal. A Chem. 237 (2005) 132–136.
[72] A.R. Derk, B. Li, S. Sharma, G.M. Moore, E.W. McFarland, H. Metiu, Methane oxidation by lanthanum oxide doped with Cu, Zn, Mg, Fe, Nb, Ti, Zr, or Ta: The connection between the activation energy and the energy of oxygen-vacancy formation, Catal. Lett. 143 (2013) 406–410.
[73] A.A. Latimer, A.R. Kulkarni, H. Aljama, J.H. Montoya, J.S. Yoo, C. Tsai, F. Abild-Pedersen, F. Studt, J.K. Nørskov, Understanding trends in C-H bond activation in heterogeneous catalysis, Nat. Mater. 16 (2017) 225–229.
[74] Y. Xiao, X. Zheng, X. Chen, L. Jiang, Y. Zheng, Synthesis of Mg-doped ordered mesoporous Pd-Al2O3 with different basicity for CO, NO, and HC elimination, Ind. Eng. Chem. Res. 56 (2017) 1687–1695.
[75] O. Demoulin, G. Rupprechter, I. Seunier, B. Le Clef, M. Navez, P. Ruiz, Investigation of parameters influencing the activation of a Pd/γ-alumina catalyst during mèthane combustion, J. Phys. Chem. B 109 (2005) 20454–20462.
[76] D. Thompsett, J. Blum, G. Jones, L. Mantarosie, J. Mugo, N. Muresan, A. Raj, The role of PdO particle size and support type on the oxidation of CH4 under dry and wet lean conditions, in: Proceedings of the Twenty Fifth North American Catalysis Society Meeting, Chicago, 2019.
[77] K. Murata, J. Ohyama, Y. Yamamoto, S. Arai, A. Satsuma, Methane combustion over Pd/Al2O3 catalysts in the presence of water: effects of Pd particle size and alumina crystalline phase, ACS Catal. 10 (2020) 8149–8156.
[78] H. Lieske, J. Völter, Pd redispersion by spreading of PdO in O2 treated Pd/Al2O3, J. Phys. Chem. 89 (1985) 1841–1842.
[79] V. Ferrer, A. Moronta, J. Sánchez, R. Solano, S. Bernal, D. Finol, Effect of the reduction temperature on the catalytic activity of Pd-supported catalysts, Catal. Today 107–108 (2005) 487–492.
[80] N.K. Nag, A study on the formation of palladium hydride in a carbon-supported palladium catalyst, J. Phys. Chem. B 105 (2001) 5945–5949.
[81] M. Delage, B. Didillon, Y. Huiban, J. Lynch, D. Uzio, Highly dispersed Pd based catalysts for selective hydrogenation reactions, Stud. Surf. Sci. Catal. 130 B (2000) 1019–1024.
[82] J.J. Chen, E. Ruckenstein, Role of interfacial phenomena in the behavior of alumina-supported palladium crystallites in oxygen, J. Phys. Chem. 85 (1981) 1606–1612.
[83] M. Moses-DeBusk, S. Sinha Majumdar, J.A. Pihl, Hydrothermally Stable Methane Oxidation Catalyst, U.S. Patent Application No. 17/739,263, Filed 05/09/2022, 2022.
[84] C. Chapon, C.R. Henry, A. Chemam, Formation and characterization of small Pd particles deposited On MgO as a model catalyst, Surf. Sci. 162 (1985) 747–754.
[85] P. Briot, M. Primet, Catalytic oxidation of methane over palladium supported on alumina, Appl. Catal. 68 (1991) 301–314.
[86] J. Bin Lim, D. Jo, S.B. Hong, Palladium-exchanged small-pore zeolites with different cage systems as methane combustion catalysts, Appl. Catal. B 219 (2017) 155–162.